Spectroscopic properties of luminous Ly α emitters at z ≈ 6-7 and comparison to the Lyman-break population

Matthee, J.J.A.; Serrano Goncalves Sobral, D.R.; Darvish, B.; Santos, S.; Mobasher, B.; Paulino-Afonso, A.; ... ; Alegre, L.

Monthly Notices of the ROYAL ASTRONOMICAL SOCIETY

MNRAS **472,** 772–787 (2017) doi:10.1093/mnras/stx2061
Advance Access publication 2017 August 12

Spectroscopic properties of luminous Ly α emitters at $z \approx 6$–7 and comparison to the Lyman-break population

Jorryt Matthee,[1]★ David Sobral,[1,2] Behnam Darvish,[3] Sérgio Santos,[2] Bahram Mobasher,[4] Ana Paulino-Afonso,[5,6] Huub Röttgering[1] and Lara Alegre[5,6]

[1]*Leiden Observatory, Leiden University, PO Box 9513, NL-2300 RA Leiden, The Netherlands*
[2]*Department of Physics, Lancaster University, Lancaster LA1 4YB, UK*
[3]*Cahill Center for Astrophysics, California Institute of Technology, 1216 East California Boulevard, Pasadena, CA 91125, USA*
[4]*University of California, Riverside, 900 University Ave, Riverside, CA 92521, USA*
[5]*Instituto de Astrofísica e Ciências do Espaço, Universidade de Lisboa, OAL, Tapada da Ajuda, PT1349-018 Lisboa, Portugal*
[6]*Departamento de Física, Faculdade de Ciências, Universidade de Lisboa, Edifício C8, Campo Grande, PT1749-016 Lisbon, Portugal*

Accepted 2017 August 8. Received 2017 August 8; in original form 2017 June 20

ABSTRACT

We present spectroscopic follow-up of candidate luminous Ly α emitters (LAEs) at $z = 5.7$–6.6 in the SA22 field with VLT/X-SHOOTER. We confirm two new luminous LAEs at $z = 5.676$ (SR6) and $z = 6.532$ (VR7), and also present *HST* follow-up of both sources. These sources have luminosities $L_{\mathrm{Ly}\,\alpha} \approx 3 \times 10^{43}$ erg s^{-1}, very high rest-frame equivalent widths of EW$_0 \gtrsim$ 200 Å and narrow Ly α lines (200–340 km s^{-1}). VR7 is the most UV-luminous LAE at $z > 6.5$, with $M_{1500} = -22.5$, even brighter in the UV than CR7. Besides Ly α, we do not detect any other rest-frame UV lines in the spectra of SR6 and VR7, and argue that rest-frame UV lines are easier to observe in bright galaxies with low Ly α equivalent widths. We confirm that Ly α line widths increase with Ly α luminosity at $z = 5.7$, while there are indications that Ly α lines of faint LAEs become broader at $z = 6.6$, potentially due to reionization. We find a large spread of up to 3 dex in UV luminosity for $>L^\star$ LAEs, but find that the Ly α luminosity of the brightest LAEs is strongly related to UV luminosity at $z = 6.6$. Under basic assumptions, we find that several LAEs at $z \approx 6$–7 have Ly α escape fractions $\gtrsim 100$ per cent, indicating bursty star formation histories, alternative Ly α production mechanisms, or dust attenuating Ly α emission differently than UV emission. Finally, we present a method to compute ξ_{ion}, the production efficiency of ionizing photons, and find that LAEs at $z \approx 6$–7 have high values of $\log_{10}(\xi_{\mathrm{ion}}/\mathrm{Hz\ erg^{-1}}) \approx 25.51 \pm 0.09$ that may alleviate the need for high Lyman-Continuum escape fractions required for reionization.

Key words: galaxies: evolution – galaxies: high-redshift – dark ages, reionization, first stars – cosmology: observations.

1 INTRODUCTION

Observations of galaxies in the early Universe help to constrain the properties of the first stellar populations and black holes and to understand the reionization process and sources responsible for that. However, because of their high redshift, these galaxies are very faint and their rest-frame spectral features (i.e. UV lines) shift to near-infrared wavelengths. This makes spectroscopic observations challenging and currently limited to the brightest sources. Therefore, it has only been possible to study a few galaxies in detail (e.g. Ouchi et al. 2013; Sobral et al. 2015; Stark et al. 2015a,b; Zabl et al. 2015). Most of these galaxies are strong Ly α (Ly α, $\lambda_{0,\,\mathrm{vac}} = 1215.7$ Å) emitters (LAEs). This is partly by selection, as LAEs can easily be identified with wide-field narrow-band surveys (e.g. Konno et al. 2014; Matthee et al. 2015) and are easier to follow-up spectroscopically, but also because the fraction of UV-bright galaxies with strong Ly α emission increases with redshift (e.g. Curtis-Lake et al. 2012; Stark et al. 2017), such that a large fraction of Lyman-break galaxies (LBGs) at $z \approx 5 - 6$ (after reionization) are typically also classed as LAEs (e.g. Pentericci et al. 2011; Stark, Ellis & Ouchi 2011; Cassata et al. 2015), see e.g. Dayal & Ferrara (2012) for a theoretical perspective.

Ly α photons undergo resonant scattering by neutral hydrogen resulting in significant uncertainties when using Ly α luminosities to study intrinsic properties of galaxies (e.g. Hayes 2015). The

★ E-mail: matthee@strw.leidenuniv.nl

fraction of observed Ly α photons depends on the spatial distribution of neutral hydrogen and the characteristics of the emitter (e.g. Matthee et al. 2016; Sobral et al. 2017). Hence, high-resolution measurements of the Ly α line profile and measurements of the extent of Ly α can provide information on the properties of both the inter-stellar medium (ISM) and the circum-galactic medium (CGM) (e.g. Møller & Warren 1998; Steidel et al. 2011; Verhamme et al. 2015; Arrigoni Battaia et al. 2016; Gronke & Dijkstra 2016). Furthermore, the prevalence of Ly α emitters and the Ly α equivalent width (EW) distribution can be used to study the neutral fraction of the inter-galactic medium (IGM) in the epoch of reionization (e.g. Dijkstra 2014; Hutter et al. 2014).

Several observations of LAEs indicate an increasingly neutral fraction at $z > 6.5$: at fixed UV luminosity, the fraction of typical LBGs with strong Ly α emission (observed in a slit) is observed to decrease with redshift (e.g. Pentericci et al. 2014; Tilvi et al. 2014); the observed number density of LAEs decreases at $z > 6$ (e.g. Konno et al. 2014; Matthee et al. 2015; Zheng et al. 2017), and at fixed central Ly α luminosity, there is more extended Ly α emission around faint LAEs at $z = 6.6$ than at $z = 5.7$ (Momose et al. 2014; Santos, Sobral & Matthee 2016). All these observations indicate that a relatively larger fraction of Ly α photons are scattered out of the line of sight at $z > 6.5$ than at $z < 6.5$. Hence, the galaxies that are still observed with high Ly α luminosities at $z > 7$ (e.g. Oesch et al. 2015; Zitrin et al. 2015; Schmidt et al. 2016) are likely the signposts of early ionized bubbles (e.g. Stark et al. 2017).

Matthee et al. (2015) performed a survey of LAEs at $z = 6.6$, increasing the available number of bright LAEs that allowed detailed study. Two LAEs from this sample ('CR7' and 'MASOSA') have been spectroscopically confirmed in Sobral et al. (2015). Several more recent wide-area surveys at $z = 6.6$ and $z = 6.9$ are now also identifying LAEs with similar luminosities (e.g. Hu et al. 2016; Shibuya et al. 2017; Zheng et al. 2017). CR7 and 'Himiko' (Ouchi et al. 2009) have been the subject of detailed spectroscopic studies (e.g. Ouchi et al. 2013; Sobral et al. 2015; Zabl et al. 2015; Bowler et al. 2017b), which indicate that their ISM is likely metal poor and in high ionization state. Such ISM conditions are similar to those in LAEs at $z \sim 2$–3 (e.g. Song et al. 2014; Trainor et al. 2015; Nakajima et al. 2016; Trainor et al. 2016; Hashimoto et al. 2017), although we note that the Ly α luminosities of the latter samples are typically an order of magnitude fainter. In order to obtain a comparison sample to those at $z \sim 7$, Santos et al. (2016) undertook a comparable survey at $z = 5.7$, just after the end of reionization. A major limitation is that the nature of the most luminous LAEs is currently unknown. Are they powered by active galactic nuclei (AGNs) or star formation? What are their metallicities?

In this paper, we present follow-up observations of candidate luminous LAEs at $z = 5.7$ and $z = 6.6$ using VLT/X-SHOOTER, which is a high-resolution spectrograph with a wavelength coverage of $\lambda = 0.3$–2.5 μm. We assess the interloper and success fractions and use these to update the number densities of the most luminous LAEs. We present the properties of the Ly α lines, UV continua of newly confirmed luminous LAEs, and constrain rest-frame UV nebular lines. Together with a compilation of spectroscopically confirmed LAEs and LBGs from the literature, we study the evolution of Ly α line widths between $z = 5.7$–6.6 and the relation between Ly α luminosity and UV luminosity. Finally, we explore the ionizing properties (such as the production efficiency of ionizing photons) using an empirical relation to estimate the Ly α escape fraction (e.g. Sobral et al. 2017).

The initial sample of luminous LAEs at $z = 5.7$ and $z = 6.6$, the observations and data reduction are presented in Section 2. We present the results in Section 3, which include updated number densities. In Section 4, we present the properties of newly confirmed LAEs. The properties of the sources are discussed and compared to the more general galaxy population at $z \approx 6$–7 in Section 5. This section includes a comparison of their Ly α line widths (Section 5.1), the UV line ratios to Ly α (Section 5.2) and their UV luminosity (Section 5.3). We discuss their production efficiency of ionizing photons in Section 5.3.1. Finally, we summarize our conclusions in Section 6. Throughout the paper, we use a flat Λ cold dark matter cosmology with $\Omega_M = 0.3$, $\Omega_\Lambda = 0.7$ and $H_0 = 70\,\mathrm{km\,s^{-1}\,Mpc^{-1}}$.

2 SAMPLE AND OBSERVATIONS

2.1 Sample

The target sample includes candidate luminous LAEs selected through NB816 and NB921 narrow-band imaging with Subaru/Suprime-Cam in the SA22 field over comoving volumes of $6.3 \times 10^6\,\mathrm{Mpc^3}$ and $4.3 \times 10^6\,\mathrm{Mpc^3}$ at $z = 5.7$ and $z = 6.6$ as described in Santos et al. (2016) and Matthee et al. (2015), respectively.[1] The data in the SA22 field is very wide-field, yet shallow and single-epoch, and is aimed at identifying the brightest LAEs. Even though the expected number of contaminants and transients is significant, these sources are bright enough to be confirmed (or refuted) in relatively small amounts of telescope time.

The initial potential target samples included 6 objects at $z = 5.7$ and 21 at $z = 6.6$. Before choosing the final targets to follow-up spectroscopically, we investigated the individual exposures, instead of only inspecting the final reduced NB image. Nine sources from the NB921 sample were moving solar-system objects whose position changed by ≈0.2–0.5 arcsec between individual exposures. The stacked image of these sources then resulted in a slightly extended object. Such extended objects in the NB image resemble confirmed LAEs at $z = 6.6$ (e.g. Himiko and CR7), leading to their misidentification as candidates. We note that point-like sources may however still be other types of transients/variables. Six other sources from the NB921 sample have been identified as a detector artefact in a single exposure, which coincides with positive noise peaks in the other exposure. Due to point spread function (PSF)-homogenization, these artefacts were then not identified in our visual inspections of the final stack. These checks were also performed for the NB816 candidates and were excluded already before the final analysis of Santos et al. (2016). These issues do not influence the search for LAE candidates in the fields with deeper coverage (COSMOS and UDS), as those fields have been observed with many more individual exposures. The final selection results in a sample of six LAE candidates at $z = 5.7$ and 6 at $z = 6.6$, all in the SA22 field (see Table 1).

2.2 Observations

We observed the candidate LAEs with the X-SHOOTER echelle spectrograph, mounted on UT2 of the VLT (Vernet et al. 2011). X-SHOOTER simultaneously takes a high-resolution spectrum with a UVB, VIS and a NIR arm, providing a wavelength coverage from 300 to 2480 nm.

[1] This sample already included the confirmed LAEs Himiko (Ouchi et al. 2013), MASOSA and CR7 (Sobral et al. 2015). It furthermore includes 14 other spectroscopically confirmed LAEs at $z = 6.6$ from Ouchi et al. (2010) and 46 spectroscopic confirmed LAEs at $z = 5.7$ from Ouchi et al. (2008), Hu et al. (2010) and Mallery et al. (2012).

Table 1. Targeted sample of LAE candidates at $z = 5.7$–6.6. Candidates selected in NB816 are from Santos et al. (2016), while candidates selected in NB921 are from Matthee et al. (2015). $L_{\mathrm{Ly}\,\alpha}$ is the estimated Ly α luminosity from NB imaging. We also list the observation dates from ESO programme ID 097.A-0943, the total on-source exposure times and the telluric standard stars that have been used for flux calibration. The final column identifies the classification of the targets, with 1 = Ly α, 2 = [O III], 3 = transient and 4 = star. Sources that are confirmed spectroscopically as Ly α emitters are shown in bold. We provide flux calibrated reduced spectra of SR6 and VR7 with the published version of the paper.

ID	RA (J2000)	Dec. (J2000)	$L_{\mathrm{Ly}\,\alpha,\,\mathrm{NB}}$ (10^{43} erg s^{-1})	Dates (2016)	$t_{\mathrm{exp,\,VIS}}$ (ks)	$t_{\mathrm{exp,\,NIR}}$ (ks)	Telluric	Class
SA22-NB816-9442	22:18:00.68	+01:04:30.53	8.4	August 5	2.92	3.12	GD153	2
SA22-NB816-366911	22:13:00.92	+00:36:24.17	4.1	August 7 and 31	5.84	6.24	GD153, EG274	3
SA22-NB816-360178	22:12:54.85	+00:32:54.76	3.8	September 3	2.92	3.12	GD71	4
SA22-NB816-390412	22:15:01.22	+00:46:24.25	3.7	August 28	5.84	6.24	Feige110	3
SR6	22:19:49.76	+00:48:23.90	3.4	September 2	5.84	6.24	GD71	1
SA22-NB816-508969	22:21:09.92	+00:47:19.52	3.3	September 3	2.92	3.12	GD71	3
VR7	22:18:56.36	+00:08:07.32	2.4	June 12, 16, July 12	8.76	9.36	GD153	1
SA22-NB921-D10845	22:18:54.82	+00:06:24.26	1.2	July 14, August 2, 3	8.76	9.36	GD153, EG274	3
SA22-NB921-W210761	22:14:38.63	+00:56:02.98	4.1	August 2	2.92	3.12	EG274	3
SA22-NB921-W219795	22:15:29.18	+00:29:17.90	3.8	August 3	2.92	3.12	EG274	3
SA22-NB921-W6153	22:20:20.79	+00:17:27.96	11.0	August 2	2.92	3.12	EG274	3
SA22-NB921-W209855	22:16:05.05	+00:51:59.23	3.8	August 3	2.92	3.12	EG274	3

Observations were done under clear skies with a seeing ranging from 0.7 to 0.9 arcsec, using 0.9 arcsec slits in the NIR and VIS arm and a slow read-out speed without binning. This leads to a spectral resolution of 1.2 Å ($R \approx 7400$) and 3.6 Å ($R \approx 4000$) in the VIS and NIR arm, respectively. We first acquired a star (with *I*-band magnitudes 16–17 AB) and applied a blind offset to the target. In order to improve the NIR sky subtraction, we use the standard `AutoNodOnSlit` procedure, which nods between two positions A and B along the slit, offset by 3.5 arcsec. This is repeated two times in an ABBA pattern. At each position, we take a 730 s exposure in the VIS arm and four 195 s exposures in the NIR arm. This results in a total exposure time of 2.92 ks in VIS and 3.12 ks in NIR in a single observing block. Several sources have been observed in two or three observing blocks, doubling or tripling the total exposure time (see Table 1).

2.3 Data reduction

Data have been reduced with the recipes from the standard X-SHOOTER pipeline (Modigliani et al. 2010), which includes corrections for the bias from read-out noise (VIS arm) and dark current (NIR arm), sky subtraction and wavelength calibration. Since wavelength calibration is done in air, we convert the wavelengths to vacuum wavelengths following Morton (1991). The standard stars GD71, GD153, EG274 and Feige110 have been observed with a 5 arcsec slit for flux calibration. We use the X-SHOOTER pipeline to combine the exposures from single observing blocks. In the case that a source has been observed with multiple observing blocks, we co-add the frames by weighting the sky background and by correcting for slight positional variations based on the position of the peak of observed Ly α lines.

2.4 Extraction

We extract 1D spectra in the VIS (NIR) arm by summing the counts in 10 (8) spatial pixels, corresponding to 1.6 (1.68) arcsec, along the wavelength direction. These extraction boxes optimize the S/N in confirmed emission-line galaxies in our data set. Slit losses are estimated by convolving the NB image to the PSF of spectroscopic observations and measuring the fraction of the flux that is retrieved within the slit compared to the flux measured with MAG-AUTO. Typical slit losses are ≈50–60 per cent. We measure the effective spectral resolution at ∼0.9 μm and ∼1.6 μm by measuring the full width at half-maximum (FWHM) of well separated, isolated skylines and find $R = 7500$ and $R = 4400$, respectively. We note that due to this high resolution, instrumental line broadening of the emission lines from the sources discussed in this paper are negligible.

The line-flux sensitivity is measured as a function of line width as follows. First, we select the sub-range of wavelengths in the collapsed 1D spectra that are within 30 nm from the targeted wavelength. Then, we measure the flux in 5000 randomly placed positions in this sub-range, with kernels corresponding to the targeted wavelength. We then calculate the noise as the rms of the 5000 measured fluxes. Note that, in the presence of skylines, this depth is a conservative estimate as it includes flux from skyline residuals, which could increase the noise by a factor of ≈2–3 depending on the specific wavelength.

3 RESULTS

3.1 NB816 targets – candidate LAEs at z = 5.7

Out of the six brightest candidate LAEs at $z = 5.7$ that we observed with X-SHOOTER, one is reliably confirmed as a Ly α emitter, one is identified as [O III] interloper, one is identified as brown dwarf star interloper and three are not detected, indicating that their NB detection was likely due to a transient or variable source (see Table 1 for a summary).

SA22-NB816-9442 is identified as an [O III] emitter at $z = 0.638$. The flux observed in NB816 can be attributed to both the 4959 and 5007 Å lines. We measure a combined line flux of $0.8 \pm 0.1 \times 10^{-16}$ erg s^{-1} cm^{-2} and observed EW >393 Å. We do not detect an emission line or continuum in the expected wavelength range or anywhere else in the spectrum of SA22-NB816-366911 and SA22-NB816-390412. This may indicate that these sources are variable/transients, as they are also not detected in any of the broad-band images. Matthee et al. (2015) confirmed two of such transients in 0.9 deg^2 of similar NB data. Hence, it is not unlikely that our selection picked up three transients in the 3.6 deg^2 coverage (see also Hibon et al. 2010).

Although we do not detect a clear emission line in the NB816 wavelength coverage in SA22-NB816-508969 and SA22-NB816-360178, we detect a faint trace of continuum in the centre of the slits.

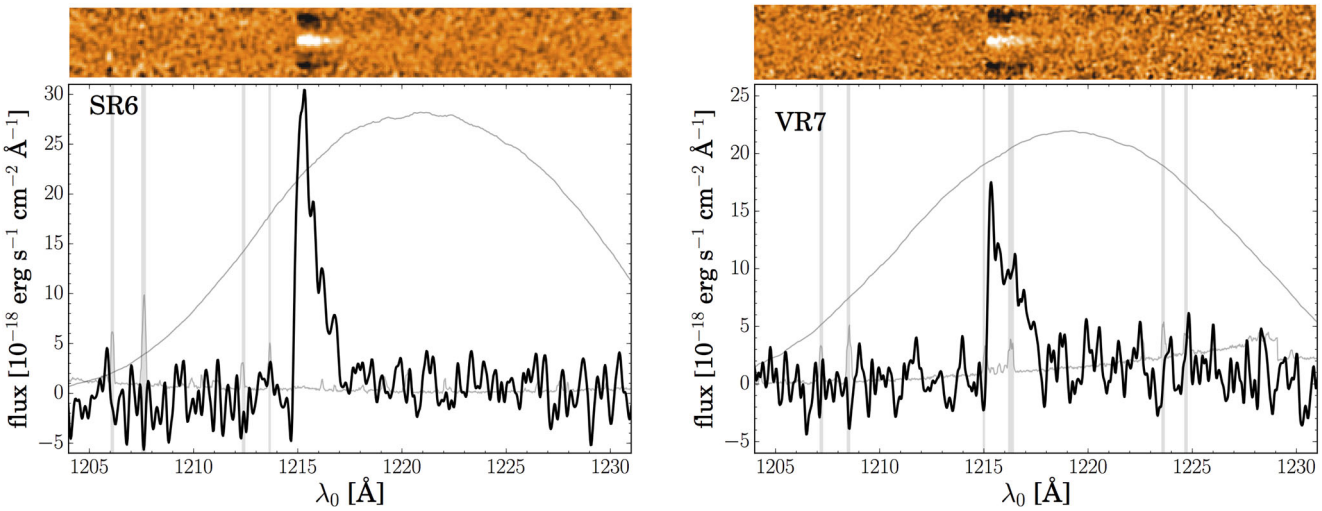

Figure 1. Rest-frame X-SHOOTER spectra of the newly confirmed luminous LAEs SR6 at $z = 5.676$ and VR7 at $z = 6.532$, zoomed in on the Ly α line. In the background, we show the NB816/NB921 filter transmission (normalized arbitrarily for visualization purposes), which illustrates that these sources are detected at ≈75 per cent and ≈92 per cent of the peak filter transmission in the original data, respectively. We also illustrate the position of atmospheric OH lines in the background, based on the noise map provided by the X-SHOOTER pipeline. The Ly α line of VR7 is slightly contaminated by a faint skyline at λ_0 ≈ 1216.3 Å (observed $\lambda \approx 9161$ Å).

For SA22-NB816-508969 this continuum is detected at low significance, making it challenging to classify the object. The continuum features, such as the peak wavelength, of SA22-NB816-360178 resemble those of a star with an effective temperature of $T \approx 3500$–3700 K, or a K or M-type star (Kurucz 1992). This interpretation is also strengthened by the point-like morphology in the available imaging.

The X-SHOOTER spectrum reliably confirms SR6[2] as a Ly α emitter at $z = 5.676 \pm 0.001$ (using the peak of Ly α), due to the asymmetric line profile (see Fig. 1) and non-detection of flux bluewards of the line. After correcting the VIS spectrum for slit losses of 56 per cent (estimated from NB imaging), we measure a line flux of $7.6 \pm 0.4 \times 10^{-17}$ erg s^{-1} cm^{-2}, consistent within the errors with the NB estimate of $9.2 \pm 1.2 \times 10^{-17}$ erg s^{-1} cm^{-2}. We also identify faint [O II] emission from a foreground source at $z = 1.322$ offset by 2.4 arcsec in the slit. We discuss the detailed properties of SR6 in Section 4.1.

3.2 NB921 targets – candidate LAEs at z = 6.6

Out of the six luminous LAE candidates at $z = 6.6$ in the SA22 field, we confirm one as an LAE, while we firmly rule out the others at the expected line fluxes from the NB921 imaging.

Based on its asymmetric line profile, the source VR7[3] is confirmed reliably as an LAE at $z = 6.532 \pm 0.001$ (corresponding to the wavelength of peak Ly α emission, see Fig. 1). After correcting for an estimated 54 per cent of slit losses, we measure a line flux of $4.9 \pm 0.5 \times 10^{-17}$ erg s^{-1} cm^{-2}, which agrees well with the NB estimate of $4.8 \pm 1.2 \times 10^{-17}$ erg s^{-1} cm^{-2}. We present detailed properties of this source in Section 4.2.

We do not detect an emission line or a continuum feature in the VIS spectra of SA22-NB921-D10845, SA22-NB921-W210761, SA22-NB921-W219795, SA22-NB921-W6153 or SA22-NB921-W209855 (see Table 1 for a summary). We measure the sensitivity of the spectra as a function of redshift and velocity width of the line. For a line width of 200 km s^{-1}, the 1σ limiting flux for wavelengths within the NB921 filter is ≈4.5(3.2) $\times 10^{-18}$ erg s^{-1} cm^{-2} for sources observed with 1 (2) observing blocks (see Table 1). The sensitivity decreases by a factor of ≈3 for a line width of 600 km s^{-1}. However, even with such broad lines, the expected line fluxes estimated from NB imaging would have been detected at the $>3\sigma$ level. This means that these sources are likely transients (note that Matthee et al. 2015 estimated that ∼6 transients were likely to be found within their sample), and that we can confidently rule out these six sources as Ly α emitters at $z = 6.6$. Therefore, our results agree very well with the estimates from Matthee et al. (2015) on the fraction of transient interlopers.

3.3 Updated number densities of the most luminous LAEs at z ≈ 6–7

Based on the spectroscopic follow-up, we provide a robust update on the number densities of luminous LAEs at $z = 5.7$–6.6 and compare those with Santos et al. (2016). At $z = 5.7$, the number density of LAEs with $L_{\mathrm{Ly}\,\alpha} = 10^{43.6 \pm 0.1}$ erg s^{-1} is $10^{-5.26^{+0.21}_{-0.17}}$ Mpc^{-3}, which is ≈0.25 dex lower than in Santos et al. (2016). At $z = 6.6$, we find that the number density at $L_{\mathrm{Ly}\,\alpha} = 10^{43.4 \pm 0.1}$ erg s^{-1} is $10^{-4.89^{+0.22}_{-0.15}}$ Mpc^{-3} and $10^{-5.35^{+0.49}_{-0.22}}$ Mpc^{-3} at $L_{\mathrm{Ly}\,\alpha} = 10^{43.6 \pm 0.1}$ erg s^{-1}. We note that all these number densities are consistent with the previous measurements within 1σ errors. The results here support little to no evolution in the bright end of the Ly α luminosity function between $z = 5.7$–6.6, and even little to no evolution at $L_{\mathrm{Ly}\,\alpha} \approx 10^{43.6}$ erg s^{-1} up to $z = 6.9$ (Zheng et al. 2017). After rejecting all candidate LAEs with a luminosity similar to CR7 (for which we measure a total luminosity of 8.5×10^{43} erg s^{-1} after correcting for the transmission curve of the NB921 filter), we constrain the number density of CR7-like sources to one per $\gtrsim 5 \times 10^6$ Mpc^3. Catalogues of LAEs at $z = 5.7$ and $z = 6.6$ will be publicly available with the published version of this paper, see Appendix B.

[2] SA22 Redshift 6, the brightest LAE at $z = 5.7$ in the SA22 field.
[3] Named after Vera Rubin, and chosen to resemble the name of LAE COSMOS Redshift 7 (CR7, Matthee et al. 2015), as it was the fifth (V) luminous LAE confirmed at $z \approx 6.6$ by the time of discovery.

4 PROPERTIES OF NEWLY CONFIRMED LAEs

4.1 SR6

SR6 is robustly confirmed to be a luminous Lyα emitter at $z = 5.676 \pm 0.001$ (Fig. 1). We measure a Lyα line width of $v_{\rm FWHM} = 236 \pm 16\,{\rm km\,s^{-1}}$ and Lyα luminosity of $2.7 \pm 0.2 \times 10^{43}\,{\rm erg\,s^{-1}}$. We do not detect continuum in the X-SHOOTER spectrum (with a 1σ depth of $3.0 \times 10^{-19}\,{\rm erg\,s^{-1}\,cm^{-2}\,\AA^{-1}}$, smoothed per resolution element), such that we can only provide a lower limit on the EW, which is ${\rm EW_0} \gtrsim 250$ Å. Based on Kashikawa et al. (2006), we quantify the line asymmetry with the *S*-statistic and weighted skewness parameters, for which we measure 0.69 ± 0.05 and 9.7 ± 0.8 Å, respectively, similar to other confirmed LAEs.

The foreground [O II] emitter identified in the slit at $z = 1.322 \pm 0.001$, spatially offset by 2.4 arcsec, is slightly magnifying SR6. We follow McLure et al. (2006) to compute the magnification from galaxy–galaxy lensing as follows:

$$\mu = \frac{d_{\rm proj}}{d_{\rm proj} - \theta_E}, \quad (1)$$

where μ is the magnification, $d_{\rm proj}$ is the projected separation in arcsec and θ_E the Einstein radius in arcsec. Under the assumption of a singular isothermal sphere, we compute θ_E as follows (e.g. Fort & Mellier 1994):

$$\theta_E = 30'' \left(\frac{\sigma_{\rm 1D}}{1000\ {\rm km\ s^{-1}}}\right)^2 \frac{D_{\rm ds}}{D_{\rm s}}, \quad (2)$$

where $\sigma_{\rm 1D}$ is the one-dimensional velocity dispersion of the foreground source, $D_{\rm ds}$ is the angular diameter distance from foreground source to the background source and $D_{\rm s}$ the angular diameter distance from observer to the background source. Using the measured $\sigma_{\rm 1D} = 130 \pm 20\,{\rm km\,s^{-1}}$, we estimate $\theta_{\rm E} = 0.24$ arcsec, resulting in a small magnification of $\mu = 1.1$. We note that additional magnification by other foreground sources is possible (for example by a faint source separated by ∼1 arcsec, see Fig. 2), although these sources are likely lower mass due to their faintness, resulting in a further negligible magnification. This results in a magnification corrected Lyα luminosity of $2.5 \pm 0.3 \times 10^{43}\,{\rm erg\,s^{-1}}$.

After confirming Lyα, we investigate the optical and near-infrared spectra for the presence of other emission lines in the rest-frame UV. In particular, we search for N V, C IV, He II, O III] and C III],[4] and check for any other significantly detected potential line – but we do not detect any above 3σ significance. We measure limiting line fluxes at the positions of the expected lines for a range of line widths. For a line width of ∼100–250 km s^{-1} and typical velocity offset with respect to Lyα of $-200\,{\rm km\,s^{-1}}$, we find a 2σ limit of $2.0 \times 10^{-17}\,{\rm erg\,s^{-1}\,cm^{-2}}$ for N V after correcting for the same slit losses as Lyα (corresponding to ${\rm EW_0} < 48$ Å). For the other lines (observed in the NIR slit), we estimate slit losses of 59 per cent. This assumes that these lines are emitted over the same spatial scales as Lyα. Because sources are un-detected in the NIR continuum, we cannot estimate slit losses from the continuum emission itself. As Lyα is likely emitted over a larger spatial scale (e.g. Wisotzki et al. 2016), slit losses for the other rest-UV lines may be overestimated (except potentially for C IV that is also a resonant line). Our upper limits are on the conservative side if this is indeed the case. For similar widths and offsets as N V, we measure 2σ limiting line fluxes of $(7.3, 3.6, 3.5, 3.9) \times 10^{-17}\,{\rm erg\,s^{-1}\,cm^{-2}}$ for (C IV, He II, O III], C III]), corresponding to ${\rm EW_0} <$(174, 86, 84, 93) Å, respectively. These limits are not particularly strong because all lines are either observed around strong sky OH lines or at low atmospheric transmission, but also due to our modest exposure time and conservative way of measuring noise.

[4] In vacuum, the wavelengths of these lines are N V$_{\lambda\lambda}$ = 1239, 1243 Å, C IV$_{\lambda\lambda}$ = 1548, 1551 Å, He II$_{\lambda}$ = 1640, O III]$_{\lambda\lambda}$ = 1661, 1666 Å and C III]$_{\lambda\lambda}$ = 1907, 1909 Å.

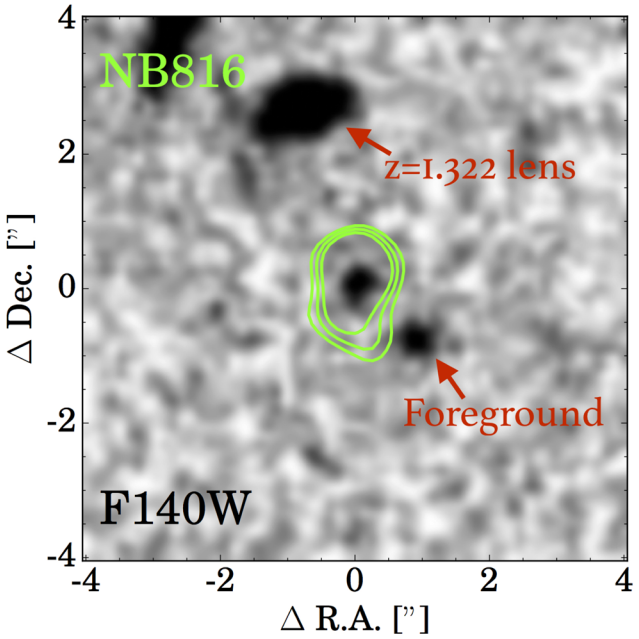

Figure 2. Rest-frame UV image of SR6 from follow-up with *Hubble Space Telescope* (*HST*; see Section 4.1.1). Green contours (at 3, 4 and 5σ level) highlight the spatial scales at which we detect Lyα emission in the NB816 filter. The background image is the F140W image, which traces rest-frame wavelengths of ∼2000 Å. We note that the PSF of the NB816 imaging is significantly larger than the F098M imaging. SR6 is clearly detected in *HST* imaging, resulting in a (magnification corrected) UV luminosity of $M_{1500} = -21.1 \pm 0.1$ based on the F098M magnitude. *HST* imaging also reveals a foreground source at ∼1 arcsec that can be identified in the ground-based optical imaging, which could slightly contribute to the flux measured in NB816, explaining why the flux inferred from the NB is slightly higher than the flux inferred from spectroscopy.

4.1.1 *HST follow-up*

We observed SR6 with our ongoing *Hubble Space Telescope (HST)*/WFC3 follow-up programme (PI: Sobral, programme 14699), and is detected in the F098M and F140W filter (see e.g. Fig. 2), with a total integration time of 4076 and 3176 s. The source is marginally resolved, consists of a single component that is separated by ≈0.2 arcsec from the peak Lyα flux. We measure magnitudes of F098M $= 25.68 \pm 0.13$ and F140W $= 25.60 \pm 0.10$ in a 0.4 arcsec aperture. Correcting for magnification, this results in $M_{1500} = -21.1 \pm 0.1$, which corresponds to a dust-uncorrected SFR $\approx 10\,{\rm M_\odot\,yr^{-1}}$ and is thus a $M^\star_{\rm UV}$ source at that redshift (Bouwens et al. 2015). Following the calibration from Schaerer et al. (2015), we estimate a stellar mass of $M_{\rm star} \approx 4 \times 10^9\,{\rm M_\odot}$. The galaxy has a moderately blue UV slope, $\beta = -1.94 \pm 0.35$. In both *HST* filters, we measure a size of $r_{1/2} = 0.8 \pm 0.2$ kpc using SExtractor (corrected for PSF broadening following, e.g. Curtis-Lake et al. 2016; Ribeiro et al. 2016). We use the *HST* photometry to estimate the continuum around Lyα and measure Lyα ${\rm EW_0} = 802 \pm 155$ Å.

Table 2. Measurements of SR6 and VR7. Luminosity and EW are measured through spectroscopy. SFR_{UV} is based on the absolute UV magnitude, assuming negligible dust attenuation and a Chabrier IMF. Stellar mass is based on UV luminosity, following a calibration based on SED models presented in Schaerer et al. (2015). ξ_{ion} is computed as described in Section 5.3.1, which assumes $f_{esc,\,Ly\,\alpha} = 100$ per cent for both sources, and is thus a lower limit. Line flux 2σ limits are in 10^{-17} erg s^{-1} cm^{-2} and EW_0 limits are in Å.

Measurement	SR6	VR7
$z_{spec,Ly\,\alpha}$	5.676 ± 0.001	6.532 ± 0.001
$L_{Ly\,\alpha}/10^{43}$ erg s^{-1}	2.5 ± 0.3	2.4 ± 0.2
$EW_{0,spec}$/Å	>250 Å	>196 Å
$EW_{0,spec+phot}$/Å	802 ± 155 Å	207 ± 10 Å
$v_{FWHM,\,Ly\,\alpha}$/km s^{-1}	236 ± 16	340 ± 14
Skewness/Å	9.7 ± 0.8	6.9 ± 0.8
M_{1500}	-21.1 ± 0.1	-22.5 ± 0.1
$SFR_{UV}/M_\odot$ yr^{-1}	10	38
$M_{star}/M_\odot$	4×10^9	1.7×10^{10}
$\log_{10}(\xi_{ion}$/Hz erg$^{-1})$	$\gtrsim 25.25 \pm 0.23$	$\gtrsim 24.66 \pm 0.17$
β	-1.94 ± 0.35	-1.97 ± 0.31
$r_{1/2}$/kpc	0.9 ± 0.1	1.7 ± 0.1
f_{NV} ($EW_{0,NV}$)	<2.0 (<48)	<1.0 (<9)
$f_{C\,IV}$ ($EW_{0,C\,IV}$)	<7.3 (<174)	<2.3 (<21)
$f_{He\,II}$ ($EW_{0,He\,II}$)	<3.6 (<86)	<2.3 (<21)
$f_{O\,III]}$ ($EW_{0,O\,III]}$)	<3.5 (<84)	<2.2 (<20)
$f_{C\,III]}$ ($EW_{0,C\,III]}$)	<3.9 (<93)	<2.1 (<19)

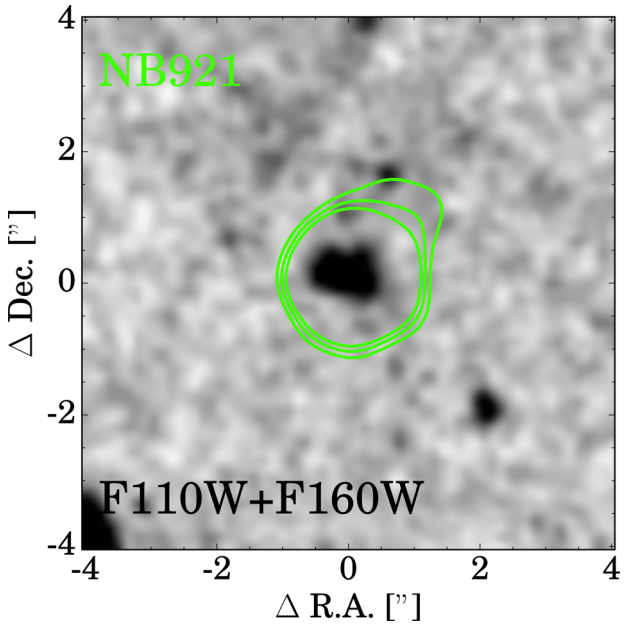

Figure 3. Rest-frame UV (F110W+F160W) image of VR7, which traces rest-frame wavelengths ∼1500 Å. The green contours show the Ly α emission measured from NB921 (at 3, 4 and 5σ level). VR7 is elongated in the UV continuum, possibly due to two merging components. The absolute UV magnitude measured within a 2 arcsec aperture centred on the Ly α peak is $M_{1500} = -22.5 \pm 0.1$ (see Section 4.2.1).

While the star formation rate (SFR), size and UV slope are typical, and not very different from UV-selected galaxies at $z \approx 6$–7 (e.g. Bowler et al. 2017a), the extremely high Ly α EW is challenging to explain with simple stellar populations (e.g. Charlot & Fall 1993), indicating an elevated production rate of ionizing photons. Such high EWs are also found in numerous other Ly α surveys (e.g. Malhotra & Rhoads 2002; Hashimoto et al. 2017), although we note that those sources are typically of fainter luminosity. High EWs may be explained by extremely low metallicity stellar populations with young ages (e.g. Schaerer 2003). Other explanations include AGN activity and contributions from cooling radiation (Rosdahl & Blaizot 2012) and shocks (Taniguchi et al. 2015). However, these processes typically result in more extended Ly α emission, which is not observed with the current observational limits. Ly α EW may also be boosted in a clumpy ISM (e.g. Duval et al. 2014; Gronke & Dijkstra 2014), but we note that measurements of the UV slope indicate little dust.

4.2 VR7

The source VR7 is a Ly α emitter at $z = 6.532 \pm 0.001$ (see Fig. 1), with a Ly α luminosity of $2.4 \pm 0.2 \times 10^{43}$ erg s^{-1}. We do not detect continuum, allowing us to place a lower limit on the equivalent width of $EW_0 > 196$ Å. The Ly α line width is $v_{FWHM} = 340 \pm 14$ km s^{-1}, the S-statistic is 0.33 ± 0.04, resulting in a Skewness of 6.9 ± 0.8 Å. This skewness is similar to those measured in fainter LAEs at $z = 6.5$ by Kashikawa et al. (2011).

We do not detect any emission line besides Ly α in the optical or near-infrared spectrum, and place the following 2σ limits (assuming line widths of ∼200 km s^{-1}, narrower than Ly α, but similar to other studies): (1.0, 2.3, 2.3, 2.2, 2.1) $\times 10^{-17}$ erg s^{-1} cm^{-2} for (N v, C iv, He ii, O iii], C iii]) (see Table 2). These error estimates are also measured including sky OH lines, even though the lines themselves may avoid skylines, and are thus conservative. Assuming a continuum level of 1.3×10^{-19} erg s^{-1} cm^{-2} Å^{-1}, these flux limits translate into EW_0 limits of <(9, 21, 21, 20, 19) Å, respectively.

4.2.1 *HST follow-up*

VR7 is detected at ≈3σ significance in the UKIDSS DXS J-band imaging ($J = 24.2$), resulting in an absolute UV magnitude of $M_{1500} = -22.5 \pm 0.2$. This luminosity places the source in the transition region between luminous galaxies and faint AGN (e.g. Willott et al. 2009; Matsuoka et al. 2016) and is ≈0.3 dex brighter than CR7 (e.g. Sobral et al. 2015). We also obtained *HST*/WFC3 imaging in the F110W and F160W filters (PI: Sobral, programme 14699), with integration times of 2612 and 5223 s. These observations reveal a relatively large-elongated galaxy ($r_{1/2} = 1.7 \pm 0.1$ kpc, elongation of 1.4), with F110W = 24.33 ± 0.09 and F160W = 24.32 ± 0.10 in a 0.6 arcsec aperture (see Fig. 3). We constrain the UV slope to $\beta = -1.97 \pm 0.31$. The UV luminosity corresponds to an SFR of 38 $M_\odot$ yr^{-1}, under the assumptions that the UV luminosity originates from star formation (as noted above, we do not detect any signs of AGN activity such as C iv or Mg ii emission at the current detection limits), a Chabrier IMF and that dust attenuation is negligible. Based on the calibration from Schaerer et al. (2015), the stellar mass is $M_{star} \approx 1.7 \times 10^{10}$ $M_\odot$. Similar to SR6, we constrain the Ly α EW using *HST* photometry and find $EW_0 = 207 \pm 10$ Å, which is higher than the typically assumed maximum EW possible due to star formation (e.g. Charlot & Fall 1993) and indicates strongly ionizing properties. Because of these properties, VR7 is an ideal target for further detailed follow-up observations.

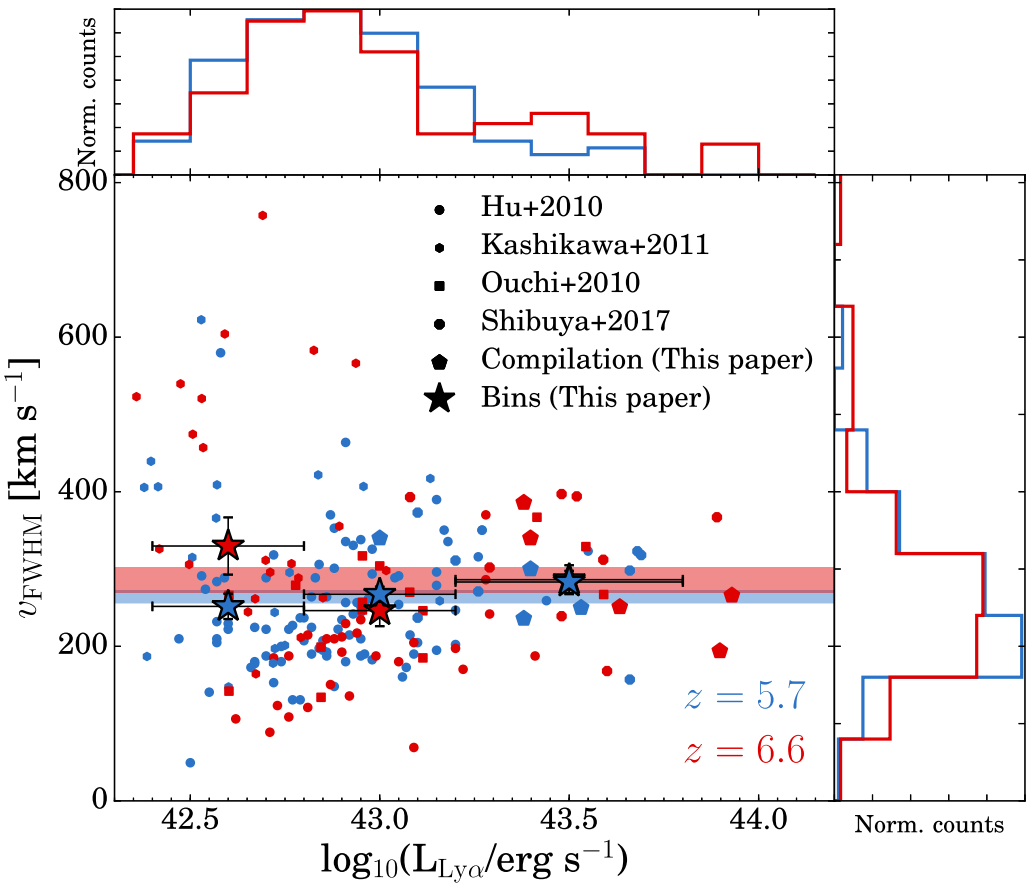

Figure 4. Ly α line widths as a function of Ly α luminosity. Blue points show LAEs at $z = 5.7$, while red points show LAEs at $z = 6.6$. The red and blue horizontal bands indicate the mean line widths and its error, while stars show the mean in bins of Ly α luminosity. At $z = 5.7$ Ly α line widths increase slightly with increasing luminosity. While the average over the full sample indicates no significant evolution in line widths from $z = 5.7$–6.6, the binned-averages indicate that line widths of faint LAEs at $z = 6.6$ are a factor of $\sim$1.2 higher than at $z = 5.7$.

5 DISCUSSION

5.1 The evolution of Ly α line widths

In order to investigate the nature of luminous LAEs at $z = 5.7$–6.6 using their Ly α line profile, we compare the measurements with a reference sample of luminous LAEs at $z \approx 2 - 3$ (Sobral et al. in preparation). These comparison sources have been selected with wide-area narrow-band surveys (e.g. Matthee et al. 2017a; Sobral et al. 2017), and we match the minimum EW$_0$ criterion to >20 Å. Even when we exclude broad-line AGN from the $z \approx 2$–3 sample, we find that luminous LAEs at $z = 5.7$–6.6 have Ly α line widths (typically 290 ± 20 km s^{-1}) that are a factor of 2–3 narrower than those at $z \approx 2$–3. These sources at lower redshift are a mix of narrow-line AGN and star-forming galaxies. This indicates that, besides non-detections of AGN-associated lines as C IV or Mg II, the Ly α lines do not clearly indicate AGN activity in luminous LAEs at $z = 5.7$–6.6.

Due to resonant scattering, the presence of neutral hydrogen broadens Ly α emission lines (e.g. Kashikawa et al. 2006; Dijkstra et al. 2014). Theoretically, Haiman & Cen (2005) show that the observed Ly α line FWHM increase mostly at faint luminosities, $L_{\rm Ly\alpha} \approx 10^{42}$ erg s^{-1}, with a more prominent evolution with higher neutral fraction and narrower intrinsic line width. Therefore, evolution in the observed Ly α profiles at $z \gtrsim 6$ may provide hints on how reionization happened. We investigate whether we find evidence for increasingly broad Ly α profiles as a function of redshift, by controlling for differences in Ly α luminosities.

In Fig. 4, we show the dependence of Ly α line width on Ly α luminosity for samples at $z = 5.7$ and $z = 6.6$. We include samples from Hu et al. (2010), Ouchi et al. (2010), Kashikawa et al. (2011), Shibuya et al. (2017) and the compilation of Ly α selected sources from Table 3, which includes the two sources confirmed in this paper. This compilation also includes the luminous LAEs at $z = 5.7$ discovered by Westra et al. (2006), studied in detail in Lidman et al. (2012), and the double-peaked LAE COLA1 at $z = 6.593$ discovered by Hu et al. (2016).[5] While there is significant scatter,

[5] In our analysis of COLA1, we find that it is detected at >5σ in the public *HST* F814W imaging (Koekemoer et al. 2007), with a magnitude of 26.2 ± 0.2. Even though the F814W filter has significant transmission above 920 nm, this magnitude indicates that a fraction of the flux density measured in F814W originates from $\lambda_0 < 1216$ Å. The F814W imaging also shows a neighbouring source within the PSF-FWHM of the NB921 imaging (data from Subaru programme S13A-057; Sobral et al. 2013), indicating that the Ly α luminosity may be overestimated. There are also $\sim$2σ detections in the *B* and *V* band Suprime-Cam images. These detections are unexpected for a source at $z = 6.6$ (because they trace below the Lyman break), and could indicate that the emission line is the [O II]$_{3727,\,3729}$ doublet at $z = 1.477$ [similar to the photometric redshift of the source in the Laigle et al. (2016)

Table 3. Compilation of Ly α line widths of spectroscopically confirmed LAEs at $5.6 < z < 6.6$ included in Fig. 4. These sources are included in Fig. 4 in addition to the spectroscopically confirmed LAEs from Hu et al. (2010), Ouchi et al. (2010), Kashikawa et al. (2011) and Shibuya et al. (2017). More detailed information on these sources is included in Table 4.

ID	Redshift	$v_{\mathrm{FWHM,\,Ly}\,\alpha}$ (km s^{-1})
SGP 8884	5.65	250 ± 30
SR6	5.67	236 ± 16
Ding-1	5.70	340 ± 100
S11 5236	5.72	300 ± 30
VR7	6.53	340 ± 14
MASOSA	6.54	386 ± 30
Himiko	6.59	251 ± 21
COLA1	6.59	194 ± 42
CR7	6.60	266 ± 15

there are some interesting results. First, the binned results indicate that line widths at $z = 5.7$ increase slightly with increasing Ly α luminosity (at $\approx 3\sigma$ significance, see also Hu et al. 2010), while this is not necessarily the case at $z = 6.6$. In order to estimate the error on the bins as conservatively as possible, we combine the formal error ($\sigma/\sqrt{N}$, where σ is the observed standard deviation and N is the number of sources in each bin) and the 1σ uncertainty on the mean estimated through bootstrap resampling the sample in the bins 1000 times in quadrature. By fitting a linear relation through the binned points at $z = 5.7$, we find that line width increases with luminosity as

$$v_{\mathrm{FWHM}} = 35^{+16}_{-13}\,\log_{10}\left(\frac{\mathrm{L_{Ly\,\alpha}}}{10^{43}\mathrm{ergs^{-1}}}\right) + 267^{+11}_{-11}\ \mathrm{km\ s^{-1}}. \quad (3)$$

Secondly, the average values in bins of Ly α luminosity indicate that LAEs with luminosities $L_{\mathrm{Ly}\,\alpha} = 10^{42.4\,-\,42.8}$ erg s^{-1} have broader line widths at $z = 6.6$ ($v_{\mathrm{FWHM}} \approx 330$ km s^{-1}) than at $z = 5.7$ ($v_{\mathrm{FWHM}} \approx 250$ km s^{-1}). We test the significance of these results by taking the uncertainties due to the limited sample size into account as follows. We bootstrap the sample in the low-luminosity bins at both $z = 5.7$ and $z = 6.6$ 1000 times and we compute the mean v_{FWHM} in each realization. The 1σ error on the mean is then the standard deviation of these 1000 measurements. At $z = 5.7$, we find $v_{\mathrm{FWHM}} = 252 \pm 17$ (error on mean) ± 112 (dispersion) km s^{-1}, while at $z = 6.6$ we find $v_{\mathrm{FWHM}} = 323 \pm 36$ (error on mean) ± 192 (dispersion) km s^{-1}. This means that the offset is only marginally significant. We also perform a Kolmogorov–Smirnov test on 1000 realizations of the sample where we have perturbed each measured v_{FWHM} with its uncertainty assuming that the uncertainty is Gaussian. We find a mean P-value of 0.12 ± 0.05 and a KS statistic of 0.27 ± 0.02. This means that the two distributions are not drawn from the same parent distribution at ≈ 85 per cent confidence level. This difference in the line widths between the samples at $z = 5.7$ and $z = 6.6$ resembles the prediction from Haiman & Cen (2005) and may be used to constrain the neutral fraction of the IGM. As the dispersion is relatively large and the difference is significant at only ≈ 85 per cent confidence level, larger samples are required to better constrain this evolution.

catalogue]. On the other hand, while the double-peak separation in the spectrum presented in Hu et al. (2016) may be explained with the [O II] doublet, the asymmetric red wing challenges this explanation. Thus, currently none of the scenarios is completely satisfactory. Follow-up observations in the NIR are required to fully distinguish between these scenarios.

The trends that Ly α line width increases slightly with luminosity at $z = 5.7$ and that the faintest LAEs may have broader Ly α lines at higher redshift may explain why neither Hu et al. (2010), Ouchi et al. (2010) or Kashikawa et al. (2011) report increasing Ly α line widths between $z = 5.7$–6.6. This is because they only studied the average overall luminosities (which does not change significantly), or probed a different Ly α luminosity regime. Interestingly, the luminosity at which line widths may increase might correspond to the luminosity where the number density (at fixed Ly α spatial scale) drops most strongly between $z = 5.7$ and 6.6 (Matthee et al. 2015), and where there is relatively more extended Ly α emission at $z = 6.6$ than at $z = 5.7$ (Santos et al. 2016). This strengthens the idea that we are witnessing the effect of patchy reionization affecting the number densities, line widths and spatial extents of faint Ly α emitters at $z = 6.6$.

5.2 UV (metal) line ratios to Ly α

As described in Section 4, no rest-UV metal lines are detected in SR6 or VR7. Such lines have also not been detected in Himiko (Zabl et al. 2015) or CR7 (Sobral et al. 2015). In this section, we explore whether this is due to the limited depth of the observations or may be attributed to any peculiar physical condition (for example due to a low metallicity). As a comparison sample, we made a compilation of UV and Ly α selected galaxies at $z \gtrsim 6$ for which limits on other UV emission lines besides Ly α are published (see Table 4). These sources have all been spectroscopically confirmed through their Ly α emission. All upper limits are converted to 2σ and we compute Ly α luminosities and absolute UV magnitudes based on the published observed magnitudes and fluxes in the case luminosities and absolute magnitudes have not been provided. We show limits on the strength of N V, C IV, He II, O III] and C III] compared to Ly α. A more detailed description on the compiled sample is provided in Appendix A. In addition, we also compare our sources with a sample of luminous LAEs at $z \approx 2 - 3$ (Sobral et al. in preparation).

Based on Table 4, it is already clear that the limits on C III] and C IV with respect to Ly α for SR6 and VR7 are higher than, or at most similar to, known detections at $z \sim 6$–7, indicating that our observations are not deep enough. As we illustrate in Fig. 5, we find that the current detections and upper limits at $z \approx 6$–7 indicate that C IV/Ly α increases towards faint UV luminosities, while it decreases or stays constant at $z \approx 2 - 3$. Contrarily, relatively high C III]/Ly α ratios are detected amongst UV bright galaxies at $z \approx 6$–7, similarly to $z \approx 2$–3. In Fig. 6, we compare the ratios of C III] and C IV to Ly α as a function of the Ly α EW$_0$. This illustrates that the $z \approx 6$–7 galaxies with observed carbon lines ubiquitously have low Ly α EWs (note that this does not necessarily mean that they are UV bright, as we showed above). This is similar to the comparison sample at $z \approx 2 - 3$ and indicates that the observability of carbon lines may actually be related strongly to the observed strength of Ly α emission and thus on the Ly α escape fraction.

We now compare the measured carbon-Ly α ratios to simple model predictions (Alegre et al. in preparation), by correcting for Ly α escape fraction empirically. The physics driving the Ly α escape fraction are complex (e.g. Hayes 2015; Henry et al. 2015), with dust, H I column density, outflows and (especially at $z > 6$) the neutral fraction of the IGM all playing an important role. However, a rough estimate of the Ly α escape fraction may be obtained from the Ly α EW$_0$, as for example shown at $z = 2.2$ in Sobral et al. (2017) [see also e.g. Yang et al. (2017) at $z \sim 0$]. Therefore, we use the EW$_0$ to provide a rough estimate of the Ly α

Table 4. Compilation of Ly α luminosities, EWs, absolute UV magnitudes and line ratios between Ly α and rest-frame UV lines. Galaxies are either categorized as Ly α (narrow-band) selected, or UV (Lyman-break) selected, and are ordered by increasing redshift (see Table A1). For the doublets C IV C III] and O III], we use the combined flux. Upper limits are at the 2σ level.

ID	$L_{\mathrm{Ly}\,\alpha}$ (erg s^{-1})	$\mathrm{EW}_{0,\mathrm{Ly}\,\alpha}$ (Å)	M_{1500} (AB)	N V/Ly α	C IV/Ly α	He II/Ly α	O III]/Ly α	C III]/Ly α
Ly α selected								
SGP 8884	3.4×10^{43}	166	–	<0.01	–	–	<0.09	<0.13
SR6	2.5×10^{43}	>250	−21.1	<0.26	<0.96	<0.47	<0.46	<0.51
Ding-3	0.7×10^{43}	62	−20.9	–	–	–	–	<0.11
Ding-4	0.2×10^{43}	106	−20.5	–	–	–	–	<0.31
Ding-5	2×10^{43}	79	−20.5	–	–	–	–	<0.05
Ding-2	0.2×10^{43}	–	−22.2	–	–	–	–	<0.31
Ding-1	1×10^{43}	21	-22.2	–	–	–	–	0.09
J233408	4.8×10^{43}	>260	>− 20.8	<0.05	0.08	<0.01	<0.01	–
S11 5236	2.5×10^{43}	160	–	<0.03	<0.13	–	<0.21	<0.18
J233454	4.9×10^{43}	217	−21.0	<0.05	<0.01	<0.01	<0.01	–
J021835	4.6×10^{43}	107	−21.7	<0.07	<0.02	<0.03	<0.01	–
WISP302	4.7×10^{43}	798	−19.6	–	–	<0.41	–	<0.29
VR7	2.4×10^{43}	>196	−22.5	<0.16	<0.36	<0.35	<0.35	<0.33
LAE SDF-LEW-1	1×10^{43}	872	>− 22	–	<0.01	<0.02	–	–
J162126	7.8×10^{43}	99	−20.5	<0.05	<0.01	<0.02	<0.01	–
J160940	1.9×10^{43}	>31	>− 22.1	<0.14	<0.19	<0.30	<0.49	–
J100550	3.9×10^{43}	>107	>− 21.5	<0.08	<0.01	<0.01	<0.03	–
J160234	3.3×10^{43}	81	−21.9	<0.11	<0.12	<0.16	<0.23	–
Himiko	4.3×10^{43}	65	−22.1	<0.03	<0.10	<0.05	–	<0.08
CR7 (recalibrated)	8.5×10^{43}	211	−22.2	<0.03	<0.12	0.14 ± 0.06	<0.09	<0.11
UV selected								
A383-5.2	0.7×10^{43}	138	–19.3	–	–	–	–	0.05 ± 0.01
RXCJ2248.7-4431-ID3	0.3×10^{43}	40	–20.1	<0.05	0.42 ± 0.12	<0.05	0.13 ± 0.04	<0.11
RXCJ2248.7–4431	0.8×10^{43}	68	−20.2	<0.48	0.45 ± 0.12	<0.28	0.31 ± 0.12	<0.09
SDF-46975	1.5×10^{43}	43	−21.5	<0.13	–	–	–	–
IOK-1	1.1×10^{43}	42	−21.3	<0.17	–	<0.12	–	–
BDF-521	1.0×10^{43}	64	−20.6	<0.26	–	<0.16	–	–
A1703_zd6	0.3×10^{43}	65	−19.3	–	0.28 ± 0.03	<0.07	0.06 ± 0.03*	–
BDF-3299	0.7×10^{43}	50	−20.6	<0.26	–	–	–	–
GLASS-stack	1×10^{43}	210−	−19.7	<0.4	<0.3	<0.2	<0.2	<0.2
EGS-zs8-2	0.5×10^{43}	9	−21.9	–	–	–	–	<0.41
FIGS_GN1_1292	0.7×10^{43}	49	−21.2	0.85 ± 0.25	–	–	–	–
GN-108036	1.5×10^{43}	33	−21.8	<0.33	–	–	–	0.09 ± 0.05
EGS-zs8-1	1.2×10^{43}	21	−22.1	–	–	–	–	0.46 ± 0.10

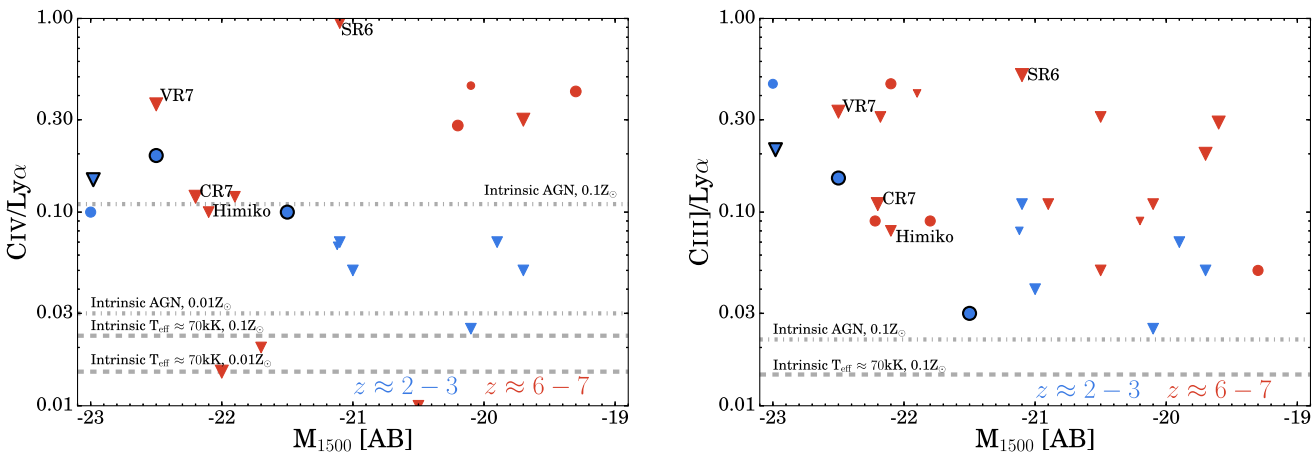

Figure 5. Observed C IV/Ly α and C III]/Lyα ratios as a function of M_{1500} for luminous LAEs at $z \approx 2$–3 (Sobral et al. in preparation) and the compilation of LAEs and LBGs at $z \approx 6$–7 from Table 4 with C IV and C III] detections and/or upper limits. Upper limits are shown with downward pointing triangles, while detections are shown with circles. We highlight AGN in the $z \approx 2$–3 sample with black edges. The symbol sizes increase with increasing Ly α EW. Horizontal lines indicate estimated intrinsic line ratios (Alegre et al. in preparation), assuming a 100 per cent Ly α escape fraction. Galaxies with C IV detections at $z \approx 6$–7 have higher C IV/Ly α ratios than LAEs at $z \approx 2 - 3$ with similar UV luminosities. The limits on CR7 and Himiko are comparable to detections of similar sources at $z \approx 2$–3, but for which an AGN nature is confirmed.

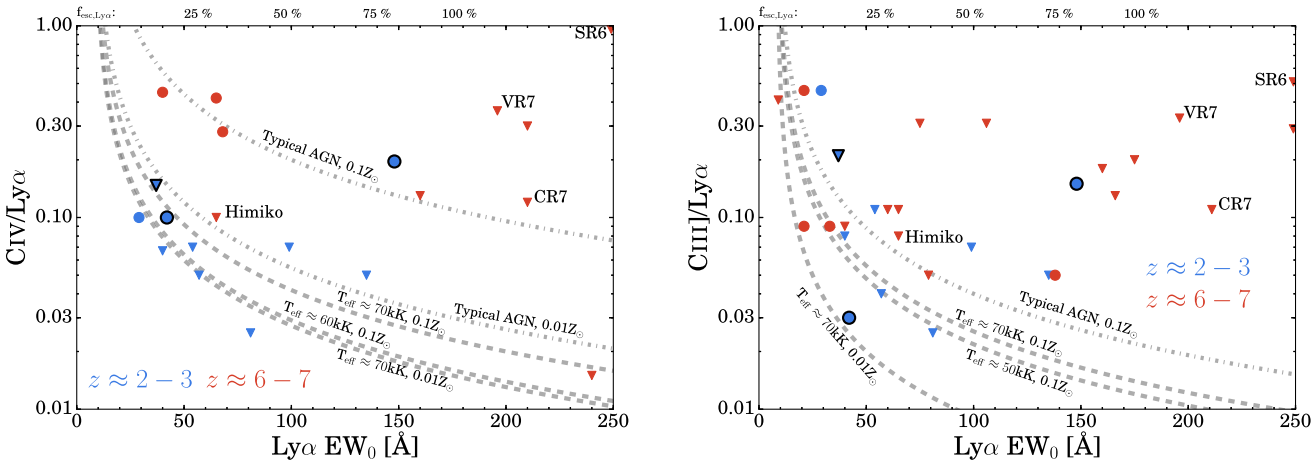

Figure 6. Observed C IV/Ly α and C III]/Ly α ratios as a function of $EW_{0,Ly\,\alpha}$ for luminous LAEs at $z \approx 2$–3 (Sobral et al. in preparation) and the compilation of LAEs and LBGs at $z \approx 6$–7 from Table 4. Upper limits are shown with downward pointing triangles, while detections are shown with circles. We highlight AGN in the $z \approx 2$–3 sample with black edges. In dashed (dot–dashed) grey lines, we show expected observed line ratios based on estimates with the star-forming (AGN) models from equation (5). It is clear that C IV and C III] are most easily observed at $z \approx 6$–7 in galaxies with relatively low Ly α EWs and that the observations of e.g. CR7 and VR7 are not deep enough.

escape fraction, and thus the intrinsic Ly α emission (that is, for example, strongly related to the ionizing emissivity). An important caveat here is that the IGM transmission decreases between $z = 2.2$–6.6 at wavelengths around Ly α (even into the red wing, Laursen, Sommer-Larsen & Razoumov 2011), such that the 'effective' Ly α escape fraction (including the effect from the IGM) may be underestimated. On the other hand, this decreasing transmission may be mitigated in the presence of galactic outflows (e.g. Dijkstra, Mesinger & Wyithe 2011). We fit the following relation to the data points from fig. 11 (right-hand panel) in Sobral et al. (2017) to estimate the escape fraction:

$$f_{esc,Ly\,\alpha} = 0.006\ EW_{Ly\,\alpha,0} - 0.05 \quad [5 < EW_{Ly\,\alpha,0} < 175], \qquad (4)$$

where $f_{esc,\,Ly\,\alpha}$ is the Ly α escape fraction. Then, we use this relation to estimate observed line ratios from their theoretically predicted values:

$$\frac{f_{C\,III]}}{f_{Ly\,\alpha}} = \frac{\alpha}{f_{esc,Ly\,\alpha}} \quad ; \quad \frac{f_{C\,IV}}{f_{Ly\,\alpha}} = \frac{\alpha}{f_{esc,Ly\,\alpha}}, \qquad (5)$$

where α is the estimated intrinsic line ratio with respect to Ly α. We use the results from CLOUDY (Ferland et al. 2013) modelling (to be presented in Alegre et al. in preparation, but with a similar approach to Feltre, Charlot & Gutkin 2016) to model the intrinsic line ratios. The sources of ionizing photons in these models are either a range of blackbodies (with temperatures ranging from 20 to 150 kK, approximating stellar populations and including populations with extreme temperature >70 kK) or a range of power laws (with spectral slopes of typical AGN), and the metallicities range from 0.001 $Z_\odot$ to solar (see also Sobral et al. in preparation). For C IV, we use models with values of α between 0.015 (for a blackbody with effective temperature ≈70 kK and a metallicity of 0.01 $Z_\odot$) and $\alpha = 0.11$ (for a typical AGN power-law slope and a metallicity 0.1 $Z_\odot$). α decreases rapidly in the case of a lower metallicity or lower effective temperatures. For C III], we use values from $\alpha = 0.005$ (T_{eff} ≈ 70 kK, Z =0.01 $Z_\odot$) to $\alpha = 0.022$ for the same AGN model as described above. The results of this modelling is shown in dashed lines in Fig. 6.

We find that current C IV detections at $z \approx 6$–7 lie closer to expected line ratios from AGN than those from star-forming galaxies (c.f. Mainali et al. 2017). However, we note that assuming a higher effective temperature of a stellar population would result in a higher C IV/Ly α ratio (compare for example the 60 kK, 0.1 $Z_\odot$ line with the 70 kK, 0.1 $Z_\odot$ line). Another issue is that Ly α luminosities from these sources are estimated from slits, such that a significant fraction may be missed due to (slightly) more extended emission. On the one hand, the detected C III]/Ly α ratios are already close to those modelled with star formation as powering source. The C IV limits observed in Himiko prefer a star-forming ionizing source, or an AGN with a very low metallicity (≈0.01 $Z_\odot$). With the current limits for SR6, CR7 and VR7 this analysis is not very meaningful, and we estimate that we would have to go a factor 5–10 deeper to detect C IV or C III].

5.3 Uv luminosities and SFRs of luminous LAEs

In order to investigate how Ly α luminosity is related to the UV luminosity, which traces SFR of time-scales of ∼100 Myr, we use near-infrared data to measure rest-frame UV luminosities (M_{1500}) for LAEs at $z = 5.7$–6.6. In addition to the new sources presented in this paper, we also add remaining candidate LAEs at $z = 5.7$–6.6 from Matthee et al. (2015) and Santos et al. (2016) and several sources from the literature as described below.

Rest-frame absolute UV magnitudes of LAEs are estimated from ground-base *Y*- and *J*-band photometry, converted to rest-frame M_{1500} at $z = 5.7$ and $z = 6.6$, respectively. *Y*-band imaging is available in the UltraVISTA (DR2) coverage of the COSMOS field (McCracken et al. 2012). *J*-band imaging is available in the UDS field through UKIDSS UDS (we use DR8; Lawrence et al. 2007), in the COSMOS field through UltraVISTA and in the SA22 field through the UKIDSS DXS. Photometry is measured in 2 arcsec apertures with SEXTRACTOR (Bertin & Arnouts 1996) in dual-image mode with the narrow-band image as detection image (i.e. the apertures are centred at the peak Ly α emission). Because the survey depth may vary from source to source (in particular in the COSMOS field due to the UltraVISTA survey design), we measure the depth locally. 2σ limits are assigned to sources that are undetected in the NIR imaging. We do not make any corrections for the fact that the effective wavelengths of the filters are not exactly at 1500 Å. However, for a typical UV slope of $\beta \approx -2.3$ (e.g. Ono et al. 2010; Jiang et al. 2013a), such a correction would only be

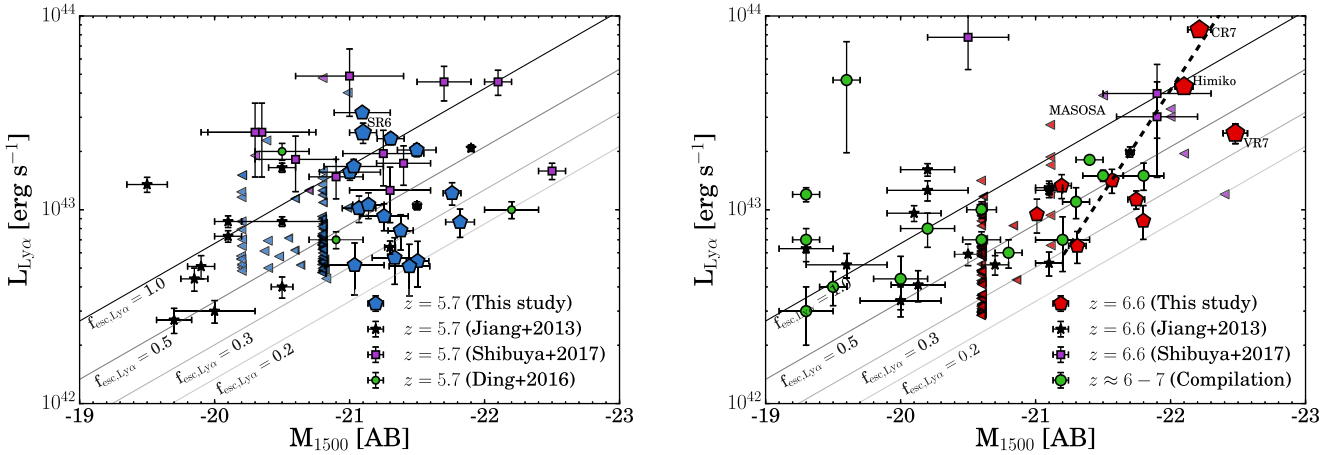

Figure 7. M_{1500} versus Ly α luminosity. Rest-frame absolute UV magnitudes are estimated from Y- and J-band photometry at $z = 5.7$ and $z = 6.6$, respectively. In the case of a non-detection, we show the local 2σ limit. Lines of constant Ly α escape fraction are computed assuming that $SFR_{UV} = SFR_{H\alpha}$, case B recombination and no attenuation due to dust. Under these assumptions, several LAEs have escape fractions >100 per cent. The sources included in this study are the LAEs from Jiang et al. (2013a), Matthee et al. (2015), Santos et al. (2016), Ding et al. (2017) and Shibuya et al. (2017) and the compilation at $z \approx$ 6–7 comprises the UV-continuum selected galaxies in Table A1 between redshifts $z = 6.1$ and $z = 7.2$ and with Ly α EW >20 Å. In the right-hand panel, the dashed line shows a fit to LAEs with $M_{1500} < -21.2$. Note that Himiko and CR7 have multiple components in the rest UV.

on the order of $\Delta M_{1500} = 0.004\,(0.03)$ for LAEs at $z = 5.7\,(6.6)$. For a more extreme blue or relative red UV slope of $\beta = -3.0$ or $\beta = -1.0$, the correction would be up to 0.1 mag. We also add the information from LAEs in the Subaru Deep Field (Kashikawa et al. 2011) that have been observed with *HST* NIR imaging by Jiang et al. (2013a), LAEs observed by Ding et al. (2017), recently spectroscopically confirmed LAEs at $z = 5.7$–6.6 by Shibuya et al. (2017) and our compilation of UV-selected galaxies between $z = 6.2$ and 7.2 with Ly α $EW_0 > 20$ Å (see Table 4, green symbols in the right-hand panel of Fig. 7). In addition to the sources from this compilation, we also added two sources from Huang et al. (2016) (see Table A1).

Fig. 7 clearly shows that at fixed Ly α luminosity, there is a large spread in UV luminosities, and vice versa (at both $z = 5.7$ and $z = 6.6$). Spectroscopically confirmed UV-selected galaxies have similar $L_{Ly\alpha}$ luminosities as LAEs. Around $L^\star$ ($L_{Ly\alpha} \approx 10^{43}$ erg s^{-1}), absolute UV magnitudes can range from up to 3 $\times M^\star_{1500}$ ($M_{1500} \approx -21.0$), down to $\approx$0.3 $\times M^\star_{1500}$, with a 1σ spread of 0.9 dex. This means that relatively shallow, wide-area Ly α surveys can be an efficient tool to select relatively UV-faint galaxies up to $z \approx 7$, thought to be signification contributors to the reionization process (e.g. Robertson et al. 2013; Faisst 2016). It also means that it is challenging to predict Ly α luminosities of UV-continuum selected galaxies, even outside the reionization epoch.

Fig. 7 also shows that there is little evidence for a relation between the Ly α luminosity and M_{1500} for Ly α-selected sources at $z = 5.7$ in our UV and Ly α luminosity range. As both M_{1500} and $L_{Ly\alpha}$ are, to first order, related to the SFR, we would have expected a correlation. To illustrate this, we show lines at constant Ly α escape fractions (based on the assumption that $SFR_{UV} = SFR_{H\alpha}$, case B recombination with $T = 10\,000$ K and $n_e = 100$ cm^{-3} and no attenuation due to dust). This result resembles the well-known Ando et al. (2006) diagram, which reveals a deficiency of luminous LAEs with bright UV magnitudes between $z \approx 5$ and 6. More recently, other surveys also revealed that the fraction of high-EW Ly α emitters increases towards fainter UV magnitudes (e.g. Schaerer, de Barros & Stark 2011; Stark, Ellis & Ouchi 2011; Cassata et al. 2015). The lack of a strong correlation between M_{1500} and $L_{Ly\alpha}$ might indicate that the SFRs are bursty (because emission-line luminosities trace SFR over a shorter time-scale than UV luminosity), or that the Ly α escape fraction is anti-correlated with M_{1500} (such that Ly α photons can more easily escape from galaxies that are fainter in the UV). A possible explanation for the latter scenario is that slightly more evolved galaxies (which are brighter in the UV) have a slightly higher dust content (e.g. Bouwens et al. 2012), affecting their Ly α luminosity more than the UV luminosity. It is interesting to note that several galaxies lie above the 100 per cent Ly α escape fraction line. This implies bursty or stochastic star formation (which is more likely in lower mass galaxies with faint UV luminosities, e.g. Mas-Ribas, Dijkstra & Forero-Romero 2016), alternative Ly α production mechanisms to star formation (such as cooling), a higher ionizing production efficiency (for example due to a top-heavy IMF or binary stars, e.g. Gotberg, de Mink & Groh 2017), or dust attenuating Ly α in a different way than the UV continuum (e.g. Neufeld 1991; Finkelstein et al. 2008; Gronke et al. 2016).

At $z = 6.6$, however, current detections indicate a relation between M_{1500} and $L_{Ly\alpha}$, albeit with significant scatter (Fig. 7). In order to be unbiased due to the depth of J-band imaging, we fit a linear relation between $\log_{10}(L_{Ly\alpha})$ and M_{1500} for LAEs with $M_{1500} < -21.2$ using a least-squares algorithm, resulting in

$$\log_{10}(L_{Ly\alpha}/\mathrm{erg\ s^{-1}}) = 20.8^{+4.2}_{-4.2} - 1.0^{+0.2}_{-0.2}\ M_{1500} \quad (6)$$

This fit indicates that for LAEs at $z \approx 6.5$–7, M_{1500} and $L_{Ly\alpha}$ are related at 5σ significance in the current data (see also Jiang et al. 2013a). We measure a (large) 1σ scatter of 0.26 dex around this relation. We note that excluding UV-selected galaxies results in a lower significance ($\approx 3.5\sigma$), but does not significantly change the fit parameters. The fitted slope between M_{1500} and $L_{Ly\alpha}$ is steeper than the slope that is expected at fixed $f_{esc,Ly\alpha}$, which could indicate that the Ly α escape fraction (or its production rate) increases towards brighter magnitudes (for Ly α-selected sources). At fainter UV luminosities, we find that the slope is consistent with being flat (within the error bars) and many of these sources only have upper limits on their UV magnitude. We also note that for a cut at high Ly α luminosity, no clear relation is seen between Ly α and UV luminosity. The presence of very luminous LAEs with luminous UV luminosities at $z = 6.6$ is at odds with the Ando et al. (2006) result, indicating additional physical processes playing a role.

We note that the most UV luminous sources at $z = 6.6$ have multiple UV components (CR7, Himiko and VR7), which could help facilitating the escape of Ly α photons. For example, outflows caused by earlier star formation episodes could boost the escape of Ly α photons through the ISM, while the same previous star formation episodes could have ionized a large enough fraction of the IGM around the galaxy such that Ly α can escape. This could be particularly important in the reionization era at $z \gtrsim 6.5$. Similarly, Jiang et al. (2013b) found that their most UV-luminous LAE at $z = 5.7$ and four out of the six LAEs with $M_{1500} < -20.5$ at $z = 6.6$ are interacting/merging. Moreover, the galaxy IOK-1, a confirmed LAE at $z = 6.96$ (Iye et al. 2006) also consists of two UV-bright components. We note that the spectroscopic follow-up presented in Furusawa et al. (2016) included two luminous UV-selected galaxies ($M_{1500} = -22.4, -22.7$) at $z \sim 7$ from Bowler et al. (2014) that have multiple components in the *HST* imaging (Bowler et al. 2017a). These sources are not detected with strong Ly α emission (with a limiting $L_{\mathrm{Ly}\,\alpha} \lesssim 3 \times 10^{42}$ erg s^{-1}), indicating that while multiple components could boost Ly α observability, they do not imply observable Ly α emission at $z \sim 7$.

5.3.1 *The production efficiency of ionizing photons*

We combine the Ly α and UV measurements to estimate ξ_{ion}, the ionizing photon production efficiency, which is an important parameter in assessing the ionizing budget from star-forming galaxies, particularly in the reionization era (e.g. Robertson et al. 2013; Bouwens et al. 2016; Matthee et al. 2017b). Under the assumption that the escape fraction of ionizing photons is close to zero, ξ_{ion} is defined as the number of produced ionizing photons per second, per unit UV magnitude:

$$\xi_{\mathrm{ion}} = \frac{Q_{\mathrm{ion}}}{L_{\mathrm{UV}}}, \tag{7}$$

where Q_{ion} is the number of emitted ionizing photons per second and L_{UV} is the UV luminosity at $\lambda_0 \approx 1500$ Å. Ideally, Q_{ion} is estimated from H α measurements, as $L_{\mathrm{H}\alpha} = 1.36 \times 10^{-12} Q_{\mathrm{ion}}$ under the assumption that $f_{\mathrm{esc,\,LyC}} = 0$ per cent (e.g. Kennicutt 1998). Unfortunately, H α measurements can only be performed at $z > 2.5$ after the launch of the *James Webb Space Telescope (JWST)*. Therefore, we use the calibration of the Ly α escape fraction with EW_0 (see equation 4), which relates the Ly α luminosity to H α luminosity under the assumption of case B recombination. Rewriting the equations results in

$$\xi_{\mathrm{ion}} = \frac{L_{\mathrm{Ly}\,\alpha}}{8.7 \times 1.36 \times 10^{-12} \times f_{\mathrm{esc,Ly}\,\alpha} \times L_{\mathrm{UV}}}. \tag{8}$$

Here, the factor of 8.7 is the case B recombination ratio between Ly α and H α under typical ISM conditions of $T_e = 10\,000$ K and $n_e = 350\,\mathrm{cm}^{-3}$ (e.g. Henry et al. 2015). $f_{\mathrm{esc,\,Ly}\,\alpha}$ is obtained through equation (4), with a maximum of 1.0 (for $\mathrm{EW}_0 \gtrsim 175$ Å). L_{UV} is computed using the measured M_{1500}, assuming negligible dust attenuation (see Bouwens et al. 2016 for a discussion on how dust attenuation affects ξ_{ion}). This empirically motivated method to estimate ξ_{ion} can easily be tested with follow-up observations with *JWST*.

Using this prescription, we calculate values of $\log_{10}(\xi_{\mathrm{ion}}/\mathrm{Hz\ erg^{-1}}) \gtrsim 25.25 \pm 0.23$ and $\gtrsim 24.66 \pm 0.17$ for SR6 and VR7, respectively. We write these as upper limits because the Ly α EWs of SR6 and VR7 indicate $f_{\mathrm{esc,\,Ly}\,\alpha} = 100$ per cent, which may be an overestimate (in the case of 50 per cent Ly α escape, ξ_{ion} would increase by 0.3 dex). For CR7 and Himiko, we measure $\log_{10}(\xi_{\mathrm{ion}}/\mathrm{Hz\ erg^{-1}}) \gtrsim 25.33 \pm 0.06$ and $\log_{10}(\xi_{\mathrm{ion}}/\mathrm{Hz\ erg^{-1}}) = 25.55 \pm 0.07$, respectively. Except for VR7, these values are similar to the measurements of faint LAEs at $z \approx 3$ (Nakajima et al. 2016) and $z \approx 4$–5 LBGs (Bouwens et al. 2016). The median value of ξ_{ion} for our compilation in Table 4 is $\log_{10}(\xi_{\mathrm{ion}}/\mathrm{Hz\ erg^{-1}}) = 25.51 \pm 0.09$ (Fig. 8), which is similar to the mean value of the reference sample of luminous LAEs at $z \approx 2$–3, for which we measure a mean $\log_{10}(\xi_{\mathrm{ion}}/\mathrm{Hz\ erg^{-1}}) = 25.45 \pm 0.05$ using the same method, and slightly lower than those measured by Schaerer et al. (2016) in a sample of low-redshift Lyman-Continuum leakers.

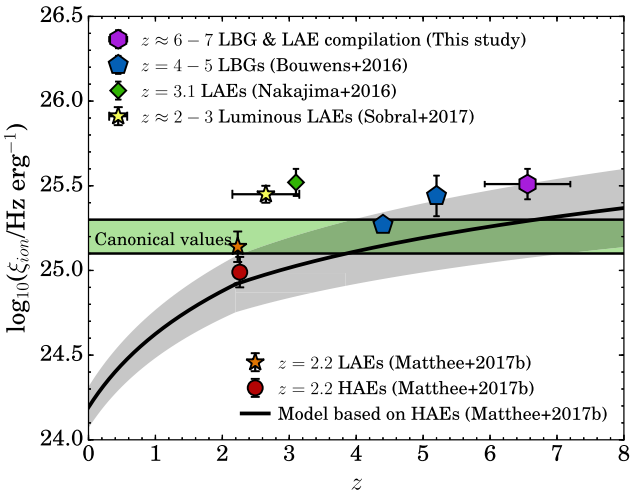

Figure 8. Production efficiency of ionizing photons (ξ_{ion}) versus redshift for different compilations of galaxies, showing our results at $z \approx 6$–7 with a purple hexagon. The green region shows the canonical values from Robertson et al. (2013). The black line shows the modelled/predicted evolution of ξ_{ion} from Matthee et al. (2017b) based on the redshift evolution of the H α EW and the relation between ξ_{ion} and H α EW for H α emitters (HAEs). It can be seen that at $z \approx 2$–3, LAEs have a significantly higher ξ_{ion} than the typical HAE/star-forming galaxy. Samples of LBGs at $z \approx 4$–5 and the compilation of LBGs and LAEs from Table 4 at $z \approx 6$–7 show elevated values of ξ_{ion} compared to the canonical value, and qualitatively confirm the trend of the modelled evolution of ξ_{ion}.

We also compare our method to the values of ξ_{ion} obtained independently by Stark et al. (2015b, 2017) using photoionization modelling of UV metal lines. While we measure a higher value of $\log_{10}(\xi_{\mathrm{ion}}/\mathrm{Hz\ erg^{-1}}) = 26.63 \pm 0.36$ for EGS-zs8-2, our results for A1703_zd6, EGS-zs-1 (see Table 4) and COS zs7-1 are $\log_{10}(\xi_{\mathrm{ion}}/\mathrm{Hz\,erg^{-1}}) = 25.52 \pm 0.18, 25.64 \pm 0.12$ and 25.63 ± 0.15, encouragingly consistent with the estimates from Stark et al. Under the model assumptions, these results indicate that luminous Ly α emitters produce ionizing photons a factor of 2 more efficiently than typically assumed (e.g. Robertson et al. 2013), and similar to the estimated ξ_{ion} based on the evolution of the H α EW/specific SFR (Matthee et al. 2017b, see Fig. 8). This implies that a significant amount of photons that reionized the Universe may have been produced in LAEs, in particular if the ISM conditions in these galaxies are also facilitating LyC photons to escape (e.g. Dijkstra et al. 2016), which can be constrained with future observations with *JWST* (e.g. Zackrisson et al. 2017).

6 CONCLUSIONS

We have presented the results of X-SHOOTER follow-up observations of a sample of luminous LAE candidates at $z = 5.7$–6.6 in the SA22 field. We present the properties of newly confirmed LAEs

(summarized in Table 2) and compare them with other LAEs and LBGs at similar redshifts. The main results are:

(i) We spectroscopically confirm SR6, the most luminous LAE at $z = 5.676$ in the SA22 field. While SR6 has a high Ly α luminosity and extreme EW ($L_{\mathrm{Ly}\,\alpha} = 2.5 \pm 0.3 \times 10^{43}$ erg s^{-1}, EW$_0 > 250$ Å), it has a typical UV continuum luminosity ($M_{1500} = -21.1 \pm 0.1$) and a narrow Ly α line (236 ± 16 km s^{-1}).

(ii) We confirm VR7, the most luminous LAE at $z = 6.532$, in the SA22 field ($\mathrm{L}_{\mathrm{Ly}\,\alpha} = 2.4 \pm 0.2 \times 10^{43}$ erg s^{-1}, EW$_0 > 196$ Å and $v_{\mathrm{FWHM}} = 340 \pm 14$ km s^{-1}, see Section 4.2). Amongst the luminous LAEs known at $z \sim 6.5$, VR7 is also the most luminous in the UV found so far ($M_{1500} = -22.5 \pm 0.2$). Despite this luminosity, we do not detect any signs of AGN activity (such as C IV or Mg II emission) in the spectrum at the current depths ($f \lesssim 2 \times 10^{-17}$ erg s^{-1} cm^{-2}, EW $\lesssim 20$ Å). In contrast, essentially all LAEs at $z \approx 2$–3 with similar Ly α and UV luminosities are AGN.

(iii) Ly α line widths increase slowly with Ly α luminosity at $z = 5.7$, while such a trend is not seen at $z = 6.6$. We find indications that the line widths of LAEs with $L_{\mathrm{Ly}\,\alpha} \approx 10^{42.5}$ erg s^{-1} increase between $z = 5.7$ and 6.6 (Section 5.1), although at relatively low statistical significance due to small sample sizes. This evolution occurs at the same luminosity where the number densities decrease, and Ly α spatial scales increase (Santos et al. 2016), all indicating patchy reionization.

(iv) In Section 5.2, we argue empirically that rest-UV lines besides Ly α are most easily observed in galaxies with relatively low Ly α EWs. This explains why carbon lines have been detected in luminous UV-continuum-selected sources, while they have not been easily detected in Ly α-selected sources.

(v) Combining our sources with a compilation of LAEs and LBGs at $z \approx 6$–7, we do not detect a clear relation between the Ly α luminosity and absolute UV magnitude at $z = 5.7$, indicating a lower Ly α escape fraction at brighter UV luminosities, for example due to dust (Section 5.3). There is a large dispersion in absolute UV magnitudes of $>L^\star$ LAEs of $\sigma = 0.9$ dex.

(vi) At $z = 6.6$, we find that, at $M_{1500} < -21$, the Ly α and UV luminosities are strongly correlated, while there is no evidence for a relation at fainter UV luminosities. This means that the Ly α escape fraction and/or its production rate increases strongly amongst luminous LAEs between $z = 5.7$ and 6.6. Most luminous LAEs show multiple components in the rest UV. This could indicate that such merging systems could boost effective Ly α transmission through the IGM at $z > 6.5$, increasing the effective Ly α escape fraction.

(vii) Under basic assumptions, we find that several LAEs at $z \approx 6$–7 would have Ly α escape fractions $\gtrsim 100$ per cent, which could indicate bursty star formation histories, alternative Ly α production mechanisms, a higher ionizing production efficiency, or dust attenuating Ly α in a different way than the UV continuum.

(viii) Using an empirical relation to estimate the Ly α escape fraction, we present a method to compute ξ_{ion}, the production efficiency of ionizing photons, based on Ly α and UV continuum measurements (Section 5.3.1). Our results indicate that luminous LAEs at $z \approx 6$–7 produce ionizing photons efficiently, with a median $\log_{10}(\xi_{\mathrm{ion}}/\mathrm{Hz\ erg^{-1}}) = 25.51 \pm 0.09$, similar to other recent measurements of LAEs and LBGs at $z \approx 2$–5. These measurements will easily be testable with *JWST*.

In the future, significant improvements can be made by observing a statistical sample of homogeneously selected Ly α emitters at $z = 5.7$–6.6 with integral field spectroscopy with *JWST*, which can measure H α up to $z = 6.6$. Such measurements can constrain any evolution in the effective Ly α escape fraction directly (due to an increasingly neutral IGM), by controlling for the apertures/spatial scales and positions of the emission (hence the IFU), and allow us to test the empirical models to estimate Ly α escape fractions and ξ_{ion}. The bright, spectroscopically confirmed LAEs are the ideal targets to pioneer such studies, as they already show extended/multiple component morphologies.

ACKNOWLEDGEMENTS

We thank the referee for a constructive report that has improved the quality and clarity of this work. The authors thank Grecco Oyarzún for discussions. JM acknowledges the support of a Huygens PhD fellowship from Leiden University. DS acknowledges financial support from the Netherlands Organisation for Scientific research (NWO) through a Veni fellowship and from Lancaster University through an Early Career Internal Grant A100679. BD acknowledges financial support from NASA through the Astrophysics Data Analysis Program (ADAP), grant number NNX12AE20G. We thank Kasper Schmidt for providing measurements. Based on observations with the W.M. Keck Observatory through programme C267D. The W.M. Keck Observatory is operated as a scientific partnership amongst the California Institute of Technology, the University of California and the National Aeronautics and Space Administration. Based on observations made with ESO Telescopes at the La Silla Paranal Observatory under programme IDs 097.A-0943, 294.A-5018 and 098.A-0819 and on data products produced by TERAPIX and the Cambridge Astronomy Survey Unit on behalf of the UltraVISTA consortium. The authors acknowledge the award of observing time (W16AN004) and of service time (SW2014b20) on the William Herschel Telescope (WHT). WHT and its service programme are operated on the island of La Palma by the Isaac Newton Group in the Spanish Observatorio del Roque de los Muchachos of the Instituto de Astrofisica de Canarias. Based on observations made with the NASA/ESA *HST*, obtained (from the Data Archive) at the Space Telescope Science Institute, which is operated by the Association of Universities for Research in Astronomy, Inc., under NASA contract NAS 5-26555. These observations are associated with programme #14699. We are grateful for the excellent data sets from the COSMOS, UltraVISTA, SXDS, UDS and CFHTLS survey teams; without these legacy surveys, this research would have been impossible. We have benefited from the public available programming language PYTHON, including the NUMPY, MATPLOTLIB, PYFITS, SCIPY and ASTROPY packages, the astronomical imaging tools SEXTRACTOR, SWARP and SCAMP and the TOPCAT analysis tool (Taylor 2013).

REFERENCES

Ando M., Ohta K., Iwata I., Akiyama M., Aoki K., Tamura N., 2006, ApJ, 645, L9
Arrigoni Battaia F., Hennawi J. F., Cantalupo S., Prochaska J. X., 2016, ApJ, 829, 3
Bagley M. B. et al., 2017, ApJ, 837, 11
Bertin E., Arnouts S., 1996, A&AS, 117, 393
Bouwens R. J. et al., 2012, ApJ, 754, 83
Bouwens R. J. et al., 2015, ApJ, 803, 34
Bouwens R. J., Smit R., Labbé I., Franx M., Caruana J., Oesch P., Stefanon M., Rasappu N., 2016, ApJ, 831, 176
Bowler R. A. A. et al., 2014, MNRAS, 440, 2810
Bowler R. A. A., Dunlop J. S., McLure R. J., McLeod D. J., 2017a, MNRAS, 466, 3612
Bowler R. A. A., McLure R. J., Dunlop J. S., McLeod D. J., Stanway E. R., Eldridge J. J., Jarvis M. J., 2017b, MNRAS, 469, 448
Cai Z. et al., 2011, ApJ, 736, L28

Cai Z., Fan X., Jiang L., Davé R., Oh S. P., Yang Y., Zabludoff A., 2015, ApJ, 799, L19
Cassata P. et al., 2015, A&A, 573, A24
Charlot S., Fall S. M., 1993, ApJ, 415, 580
Cuby J.-G., Le Fèvre O., McCracken H., Cuillandre J.-C., Magnier E., Meneux B., 2003, A&A, 405, L19
Curtis-Lake E. et al., 2012, MNRAS, 422, 1425
Curtis-Lake E. et al., 2016, MNRAS, 457, 440
Dayal P., Ferrara A., 2012, MNRAS, 421, 2568
Dijkstra M., 2014, PASA, 31, 40
Dijkstra M., Mesinger A., Wyithe J. S. B., 2011, MNRAS, 414, 2139
Dijkstra M., Wyithe S., Haiman Z., Mesinger A., Pentericci L., 2014, MNRAS, 440, 3309
Dijkstra M., Gronke M., Venkatesan A., 2016, ApJ, 828, 71
Ding J. et al., 2017, ApJ, 838, L22
Duval F., Schaerer D., Östlin G., Laursen P., 2014, A&A, 562, A52
Faisst A. L., 2016, ApJ, 829, 99
Feltre A., Charlot S., Gutkin J., 2016, MNRAS, 456, 3354
Ferland G. J. et al., 2013, Rev. Mex. Astron. Astrofis., 49, 137
Finkelstein S. L., Rhoads J. E., Malhotra S., Grogin N., Wang J., 2008, ApJ, 678, 655
Finkelstein S. L. et al., 2013, Nature, 502, 524
Fort B., Mellier Y., 1994, A&AR, 5, 239
Furusawa H. et al., 2016, ApJ, 822, 46
Gotberg Y., de Mink S. E., Groh J. H., 2017, preprint (arXiv:1701.07439)
Gronke M., Dijkstra M., 2014, MNRAS, 444, 1095
Gronke M., Dijkstra M., 2016, ApJ, 826, 14
Gronke M., Dijkstra M., McCourt M., Oh S. P., 2016, ApJ, 833, L26
Haiman Z., Cen R., 2005, ApJ, 623, 627
Hashimoto T. et al., 2017, MNRAS, 465, 1543
Hayes M., 2015, PASA, 32, e027
Henry A., Scarlata C., Martin C. L., Erb D., 2015, ApJ, 809, 19
Hibon P. et al., 2010, A&A, 515, A97
Hu E. M., Cowie L. L., Barger A. J., Capak P., Kakazu Y., Trouille L., 2010, ApJ, 725, 394
Hu E. M., Cowie L. L., Songaila A., Barger A. J., Rosenwasser B., Wold I. G. B., 2016, ApJ, 825, L7
Huang K.-H. et al., 2016, ApJ, 817, 11
Hutter A., Dayal P., Partl A. M., Müller V., 2014, MNRAS, 441, 2861
Iye M. et al., 2006, Nature, 443, 186
Jiang L. et al., 2013a, ApJ, 772, 99
Jiang L. et al., 2013b, ApJ, 773, 153
Kashikawa N. et al., 2006, ApJ, 648, 7
Kashikawa N. et al., 2011, ApJ, 734, 119
Kashikawa N. et al., 2012, ApJ, 761, 85
Kennicutt Jr R. C., 1998, ARAA, 36, 189
Koekemoer A. M. et al., 2007, ApJS, 172, 196
Konno A. et al., 2014, ApJ, 797, 16
Kurucz R. L., 1992, in Barbuy B., Renzini A., eds, IAU Proc. Symp. 149, The Stellar Populations of Galaxies. Kluwer Academic Publishers, Dordrecht, p. 225
Laigle C. et al., 2016, ApJS, 224, 24
Laursen P., Sommer-Larsen J., Razoumov A. O., 2011, ApJ, 728, 52
Lawrence A. et al., 2007, MNRAS, 379, 1599
Lidman C., Hayes M., Jones D. H., Schaerer D., Westra E., Tapken C., Meisenheimer K., Verhamme A., 2012, MNRAS, 420, 1946
Mainali R., Kollmeier J. A., Stark D. P., Simcoe R. A., Walth G., Newman A. B., Miller D. R., 2017, ApJ, 836, L14
Malhotra S., Rhoads J. E., 2002, ApJ, 565, L71
Mallery R. P. et al., 2012, ApJ, 760, 128
Mas-Ribas L., Dijkstra M., Forero-Romero J. E., 2016, ApJ, 833, 65
Matsuoka Y. et al., 2016, ApJ, 828, 26
Matthee J., Sobral D., Santos S., Röttgering H., Darvish B., Mobasher B., 2015, MNRAS, 451, 400
Matthee J., Sobral D., Oteo I., Best P., Smail I., Röttgering H., Paulino-Afonso A., 2016, MNRAS, 458, 449
Matthee J., Sobral D., Best P., Smail I., Bian F., Darvish B., Röttgering H., Fan X., 2017a, MNRAS, 471, 629
Matthee J., Sobral D., Best P., Khostovan A. A., Oteo I., Bouwens R., Röttgering H., 2017b, MNRAS, 465, 3637
McCracken H. J. et al., 2012, A&A, 544, A156
McLure R. J. et al., 2006, MNRAS, 372, 357
Modigliani A. et al., 2010, in Silva D. R., Peck A. B., Soifer B. T., eds, Proc. SPIE Conf. Ser. Vol. 7737, Observatory Operations: Strategies, Processes, and Systems III. SPIE, Bellingham, p. 773728
Momose R. et al., 2014, MNRAS, 442, 110
Morton D. C., 1991, ApJS, 77, 119
Møller P., Warren S. J., 1998, MNRAS, 299, 661
Nakajima K., Ellis R. S., Iwata I., Inoue A. K., Kusakabe H., Ouchi M., Robertson B. E., 2016, ApJ, 831, L9
Neufeld D. A., 1991, ApJ, 370, L85
Oesch P. A. et al., 2015, ApJ, 804, L30
Ono Y., Ouchi M., Shimasaku K., Dunlop J., Farrah D., McLure R., Okamura S., 2010, ApJ, 724, 1524
Ono Y. et al., 2012, ApJ, 744, 83
Ouchi M. et al., 2005, ApJ, 635, L117
Ouchi M. et al., 2008, ApJS, 176, 301
Ouchi M. et al., 2009, ApJ, 696, 1164
Ouchi M. et al., 2010, ApJ, 723, 869
Ouchi M. et al., 2013, ApJ, 778, 102
Pentericci L. et al., 2011, ApJ, 743, 132
Pentericci L. et al., 2014, ApJ, 793, 113
Ribeiro B. et al., 2016, A&A, 593, A22
Richard J., Kneib J.-P., Ebeling H., Stark D. P., Egami E., Fiedler A. K., 2011, MNRAS, 414, L31
Robertson B. E. et al., 2013, ApJ, 768, 71
Rosdahl J., Blaizot J., 2012, MNRAS, 423, 344
Santos S., Sobral D., Matthee J., 2016, MNRAS, 463, 1678
Schaerer D., 2003, A&A, 397, 527
Schaerer D., de Barros S., Stark D. P., 2011, A&A, 536, A72
Schaerer D., Boone F., Zamojski M., Staguhn J., Dessauges-Zavadsky M., Finkelstein S., Combes F., 2015, A&A, 574, A19
Schaerer D., Izotov Y. I., Verhamme A., Orlitová I., Thuan T. X., Worseck G., Guseva N. G., 2016, A&A, 591, L8
Schmidt K. B. et al., 2016, ApJ, 818, 38
Schmidt K. B. et al., 2017, ApJ, 839, 17
Shibuya T. et al., 2017, preprint (arXiv:1705.00733)
Shimasaku K. et al., 2006, PASJ, 58, 313
Sobral D., Smail I., Best P. N., Geach J. E., Matsuda Y., Stott J. P., Cirasuolo M., Kurk J., 2013, MNRAS, 428, 1128
Sobral D., Matthee J., Darvish B., Schaerer D., Mobasher B., Röttgering H. J. A., Santos S., Hemmati S., 2015, ApJ, 808, 139
Sobral D. et al., 2017, MNRAS, 466, 1242
Song M. et al., 2014, ApJ, 791, 3
Stark D. P., Ellis R. S., Ouchi M., 2011, ApJ, 728, L2
Stark D. P. et al., 2015a, MNRAS, 450, 1846
Stark D. P. et al., 2015b, MNRAS, 454, 1393
Stark D. P. et al., 2017, MNRAS, 464, 469
Steidel C. C., Bogosavljević M., Shapley A. E., Kollmeier J. A., Reddy N. A., Erb D. K., Pettini M., 2011, ApJ, 736, 160
Taniguchi Y. et al., 2015, ApJ, 809, L7
Taylor M., 2013, Starlink User Note, 253
Tilvi V. et al., 2014, ApJ, 794, 5
Tilvi V. et al., 2016, ApJ, 827, L14
Trainor R. F., Steidel C. C., Strom A. L., Rudie G. C., 2015, ApJ, 809, 89
Trainor R. F., Strom A. L., Steidel C. C., Rudie G. C., 2016, ApJ, 832, 171
Vanzella E. et al., 2011, ApJ, 730, L35
Vanzella E. et al., 2017, ApJ, 842, 47
Verhamme A., Orlitová I., Schaerer D., Hayes M., 2015, A&A, 578, A7
Vernet J. et al., 2011, A&A, 536, A105
Westra E. et al., 2006, A&A, 455, 61
Willott C. J. et al., 2009, AJ, 137, 3541
Willott C. J. et al., 2013, AJ, 145, 4
Wisotzki L. et al., 2016, A&A, 587, A98
Yang H. et al., 2017, ApJ, 844, 171

Zabl J., Nørgaard-Nielsen H. U., Fynbo J. P. U., Laursen P., Ouchi M., Kjærgaard P., 2015, MNRAS, 451, 2050
Zackrisson E. et al., 2017, ApJ, 836, 78
Zheng Z.-Y. et al., 2017, ApJ, 842, L22
Zitrin A. et al., 2015, ApJ, 810, L12

SUPPORTING INFORMATION

Supplementary data are available at *MNRAS* online.

SUPPLEMENT.zip

Please note: Oxford University Press is not responsible for the content or functionality of any supporting materials supplied by the authors. Any queries (other than missing material) should be directed to the corresponding author for the article.

APPENDIX A: GALAXY COMPILATION

Here, we describe shortly the details of the sample of sources listed in Table A1. Part of this sample are narrow-band selected LAEs, where the Ly α flux is measured with a NB (except for WISP302, which is measured with the HST/WFC3 grism, Bagley et al. 2017). The other part of the sample are UV-selected LBGs for which the Ly α flux and EW have been measured from slit spectroscopy, except for the grism measurements of RXCJ2248.7-4431 (Schmidt et al. 2017), the GLASS-stack (Schmidt et al. 2016) and FIGS_GN1_1292 (Tilvi et al. 2016). We note that due to extended Ly α emission and slit losses their Ly α luminosities may be underestimated, in particular when Ly α is offset from the UV emission (e.g. Vanzella et al. 2017). For CR7, we use updated constraints on metal lines from the recalibrated spectrum that will be presented in Sobral et al. (in preparation).

In the case Ly α luminosities are not published, we have computed them from the published line flux and luminosity distance corresponding to the source redshift. For sources from Ding et al. (2017), we have used luminosities from their discovery papers (Ouchi et al. 2005; Shimasaku et al. 2006). If not published, M_{1500} is computed based on the observed magnitude in the band closest to a rest-frame $\lambda = 1500$ Å, corrected for the distance modulus and bandwidth spreading and for possible lensing magnification. In the case of emission-line doublets (such as C III]$_{1907,\,1909}$), we use the sum of both lines, except in the case of the O III] doublet of A1703_zd6, where only one component is measured due to adjacent skylines. Most measurements of/limits on rest-UV lines besides Ly α and N V have been performed with slit spectroscopy from the ground and

Table A1. Galaxies included in compilations of line widths and rest-UV line ratios.

ID	Redshift	Reference
Ly α selected		
SGP 8884	5.65	Westra et al. (2006); Lidman et al. (2012)
SR6	5.676	**This paper**
Ding-3	5.69	Ouchi et al. (2005); Ding et al. (2017)
Ding-4	5.69	Ouchi et al. (2005); Ding et al. (2017)
Ding-5	5.69	Ouchi et al. (2005); Ding et al. (2017)
Ding-2	5.692	Ouchi et al. (2005); Ding et al. (2017)
Ding-1	5.70	Shimasaku et al. (2006); Ding et al. (2017)
J233408	5.707	Shibuya et al. (2017)
S11 5236	5.72	Westra et al. (2006); Lidman et al. (2012)
J233454	5.732	Shibuya et al. (2017)
J021835	5.757	Shibuya et al. (2017)
WISP302	6.44	Bagley et al. (2017)
VR7	6.532	**This paper**
LAE SDF-LEW-1	6.538	Kashikawa et al. (2012)
J162126	6.545	Shibuya et al. (2017)
J160940	6.564	Shibuya et al. (2017)
J100550	6.573	Shibuya et al. (2017)
J160234	6.576	Shibuya et al. (2017)
Himiko	6.59	Ouchi et al. (2009); Zabl et al. (2015)
COLA1	6.593	Hu et al. (2016)
CR7	6.604	Sobral et al. (2015)
UV selected		
WMH S	5.618	Willott et al. (2013)
WMH 13	5.983	Willott et al. (2013)
A383-5.2	6.0294	Richard et al. (2011); Stark et al. (2015a)
WMH 5	6.068	Willott et al. (2013)
RXCJ2248.7-4431-ID3	6.11	Mainali et al. (2017)
RXCJ2248.7-4431	6.11	Schmidt et al. (2017)
CLM 1	6.17	Cuby et al. (2003)
MACS0454-1251	6.32	Huang et al. (2016)

Table A1 – *continued*

ID	Redshift	Reference
RXJ1347-1216	6.76	Huang et al. (2016)
SDF-46975	6.844	Ono et al. (2012)
IOK-1	6.96	Iye et al. (2006); Cai et al. (2011); Ono et al. (2012)
BDF-521	7.01	Vanzella et al. (2011); Cai et al. (2015)
A1703_zd6	7.045	Stark et al. (2015b)
BDF-3299	7.109	Vanzella et al. (2011)
GLASS-stack	<7.2 >	Schmidt et al. (2016)
GN-108036	7.213	Ono et al. (2012); Stark et al. (2015a)
EGS-zs8-2	7.477	Stark et al. (2017)
FIGS_GN1_1292	7.51	Finkelstein et al. (2013); Tilvi et al. (2016)
EGS-zs8-1	7.73	Oesch et al. (2015); Stark et al. (2017)

are thus significantly hampered by the sky OH emission lines in the near-infrared. This is less of an issue for grism data, although these are limited by their spectral resolution, and thus mostly sensitive to high-EW lines. Another employed technique used a matched narrow-band that measures specific emission lines at specific redshifts, for example C III] at $z = 5.7$ (Cai et al. 2011, 2015; Ding et al. 2017).

APPENDIX B: CATALOGUES OF CANDIDATE LAES AT $z = 5.7$–6.6

We publish catalogues of all candidate LAEs at $z = 5.7$ from Santos et al. (2016) and at $z = 6.6$ from Matthee et al. (2015) with the paper. The first five entries of these catalogues are shown in Tables B1 and B2.

Table B1. First five entries of our candidate LAEs at $z = 5.7$ from Santos et al. (2016). Full electronic table is available online. Line-flux ($f_{\rm NB816}$), Ly α luminosity (assuming a luminosity distance corresponding to $z = 5.7$) and EW_0 are measured in 2 arcsec apertures. For sources with spectroscopically confirmed redshift, we corrected the luminosity for the narrow-band filter transmission at the wavelength where the line is observed.

ID	RA (J2000)	Dec. (J2000)	$f_{\rm NB816}$ (10^{-17} erg s^{-1} cm^{-2})	$L_{\rm Ly\alpha}$ (10^{42} erg s^{-1})	EW_0 (Å)
SA22-NB816-480736	22:17:28.81	+00:53:02.29	6.6	24.6	178
SA22-NB816-444574	22:17:29.41	+00:34:13.07	2.3	8.5	27
SA22-NB816-429880	22:17:33.65	+00:26:47.99	1.4	5.1	25
SA22-NB816-429969	22:17:36.16	+00:26:49.65	3.7	13.6	380
SA22-NB816-438282	22:17:37.24	+00:30:57.20	3.9	14.3	43

Table B2. First five entries of our candidate LAEs at $z = 6.6$ from Matthee et al. (2015). Full electronic table is available online. Line-flux ($f_{\rm NB921}$), Ly α luminosity (assuming a luminosity distance corresponding to $z = 6.55$) and EW_0 are measured in 2 arcsec apertures. For sources with spectroscopically confirmed redshift, we corrected the luminosity for the narrow-band filter transmission at the wavelength where the line is observed.

ID	RA (J2000)	Dec. (J2000)	$f_{\rm NB921}$ (10^{-17} erg s^{-1} cm^{-2})	$L_{\rm Ly\alpha}$ (10^{42} erg s^{-1})	EW_0 (Å)
VR7	22:18:56.36	+00:08:07.32	4.8	23.4	203
COSMOS-NB921-20802	10:02:07.83	+02:32:17.25	1.4	7.0	56
COSMOS-NB921-5032	10:02:04.33	+02:20:29.12	2.4	11.7	125
COSMOS-NB921-107681	10:01:54.68	+02:10:18.59	2.1	10.3	100
COSMOS-NB921-100684	10:01:27.54	+02:06:46.47	3.5	17.0	116

This paper has been typeset from a TEX/LATEX file prepared by the author.